



Master's Thesis

UWB based Positioning

by

Chunguang Jiang and Jiao Pan

Department of Electrical and Information Technology
Faculty of Engineering, LTH, Lund University
SE-221 00 Lund, Sweden

Abstract

Radio-based positioning is an exciting area with various applications ranging from coarse localization using received signal strengths in cellular systems to precise localization and tracking using ultra wideband (UWB) technology. Time-based positioning systems, often based on UWB, typically need precise synchronization between target nodes and reference nodes for the position estimates. In this thesis, sensor localization using UWB signals in an unsynchronized scenario is studied. Based on the time of arrival of multipath components for different receivers, the positions of the nodes can be estimated without synchronization between them. Three outdoor measurements have been conducted. The resulting positioning errors in the centimeter range show that it is possible to do precise localization with unsynchronized nodes.

Index terms—Ultra wideband, positioning, localization, Unsynchronized Time of Arrival (UTOA), Far Field Unsynchronized Time of Arrival (FFUTOA)

Acknowledgments

First of all, we would like to express the deepest appreciation to our supervisor Dr. Fredrik Tufvesson, this research would not exist without his continuous support, encouragement and professional guidance. We are also very grateful to Dr. Ghassan Dahman for his expert guide, patience and thoughtful comments. Yubin Kuang from the Centre of Mathematical Sciences deserves a word for his assist and support.

Secondly, we would like to thank Lund University, the Department of Electrical and Information Technology, and the 2011/2013 Wireless Communications class for making the two years studying here so special.

Thirdly, a lot of thanks go to our friends here who not only lent their PCs to us, but also helped us with the midnight measurements.

Last but not the least, Chunguang wants to express his love and appreciation to his parents Yimin Song and Liang Jiang. And Jiao would like to thank her parents, Zhiming Pan and Xiaolin Rao, her dear grandma Shuhua Rao for their endless love, encouragement and support.

Chunguang Jiang
Jiao Pan

Table of Contents

Abstract	1
Acknowledgments	1
Table of Contents	i
1 Introduction	1
1.1 Ultra-Wideband Signals	2
1.2 PlusON410 Unit	5
1.3 Position Estimation Schemes	6
1.3.1 Received Signal Strength (RSS)	6
1.3.2 Time of arrival (TOA)	8
1.3.3 Time difference of Arrival (TDOA)	10
1.3.4 Angle of arrival (AOA)	11
1.4 Thesis aim	12
1.5 Thesis outline	13
2 Pre-test and verification	14
2.1 Principle of the UTOA	14
2.2 P410 configuration	16
2.2.1 Transmit configuration	17
2.2.2 Receive configuration	18
2.3 Outdoor Pre-test	21
2.4 Conclusion	24
3 Multi-unit measurement	25
3.1 non-far field 2D case	25
3.2 2D case	29
3.3 2D far field case	31
4 Position estimates	35
4.1 Position estimates of the non-far field 2D case	35
4.2 Position estimates of the 2D case	36
4.3 Position estimates of the 2D far field case	38
5 Discussions of 2D/3D far field case	40
5.1 2D/3D far field case	40
6 Conclusions and improvements	44
References	45
Appendix	48
A.1 Measured data and received signals for non-far field 2D case	48
A.1.1 Measured data	48
A.1.2 Received signals	49
A.1.3 Different distance	54
A.2 Measured data and received signals for 2D case	57

A.2.1 Measured data	57
A.2.2 Received signals.....	59
A.2.3 Different distance	63
A.3 Measured data and received signals for 2D far field case	65
A.3.1 Measured data	65
A.3.2 Received signals.....	67
A.3.3 Different distance	69
A.4 Measured data and receive signals for 2D/3D far field case	72
A.4.1 Measured data	72
A.4.2 Receive signal	73

CHAPTER 1

1 Introduction

Radio-based positioning has been an exciting area in wireless system for many years, applications can be found in various areas, such as industry, medical, sport, science and personal daily life. The increasing demands motivate rapid development of positioning technologies.

As shown in figure 1, a roughly overview of positioning systems can be divided in the following: GSM/3G cell-phone positioning, Global Positioning System (GPS), WLAN, Bluetooth local positioning systems and Ultra-wideband (UWB) systems [1].

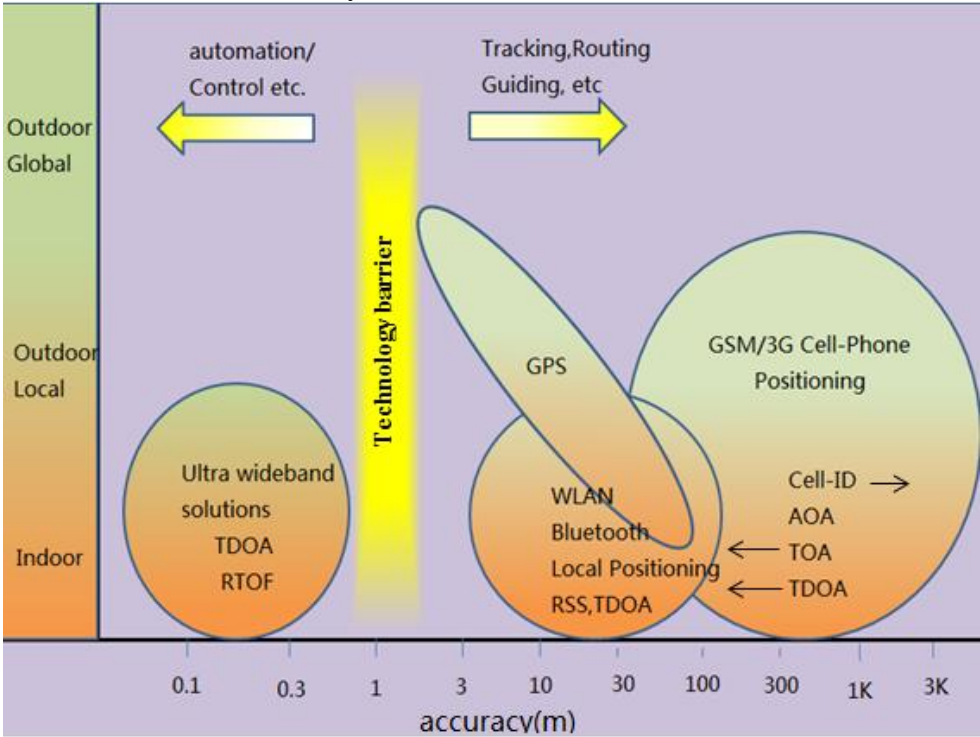


Figure 1. Overview of current wireless positioning systems [1].

GSM/3G cell phone positioning is well suited for both local (indoor/outdoor) and global situations. One solution can be identifying cell-

ID that is related to the physical position of base stations. Typically, cell size varies from hundreds of meters to several kilometers, which lead to the imprecise results. The accuracy of cell phone positioning is often not better than 100 meters [2-4].

GPS is a well known and widely used positioning system. The position of the receiver is obtained by the timepoint when the message was transmitted and the satellite position of this timepoint. It performs excellent in the outdoor cases. However, it has bad performance in some urban areas and indoor cases due to multipath or penetration losses. Therefore, GPS system has to make some improvements to satisfy the growing demands for localization in urban area and indoor environments [5].

WLAN and Bluetooth based local positioning systems are quite attractive these days. It can provide mutual synergy between the positioning and the communication systems. Compared to the cell phone positioning, it improves the accuracy to approximately to 3-30 meters [1].

The last system mentioned is UWB systems, which typically have low power consumption and large bandwidth. These latter brings significant improvement from an accuracy point of view. It is because with an appropriate bandwidth, it is of high probability that multipath transmission could be resolved and separated. Typically, this may improve accuracy down to 0.1-1 meter [1].

This paper will focus on UWB systems, which have some exciting features, as discussed later.

1.1 Ultra-Wideband Signals

Investigation and application of UWB signals started more than three decades ago [6]. UWB signals are characterized by their large bandwidth compared to conventional narrow-band/wide-band signals. A UWB signal is defined to have an absolute bandwidth of at least 500 MHz or a fractional (relative) bandwidth of larger than 20% according to the Federal Communications Commission [7, 8]. As shown in figure 2, the difference between the upper frequency f_H of the -10dB point and the lower frequency point f_L gives the absolute bandwidth

$$B = f_H - f_L, \quad (1)$$

which is also called the -10dB bandwidth. Besides, the so-called fractional bandwidth is obtained as

$$B_{frac} = \frac{B}{f_c}, \quad (2)$$

where f_c is the center frequency and is given by

$$f_c = \frac{f_H + f_L}{2}. \quad (3)$$

Consequently, the fractional bandwidth can be expressed as

$$B_{frac} = \frac{2(f_H - f_L)}{f_H + f_L}. \quad (4)$$

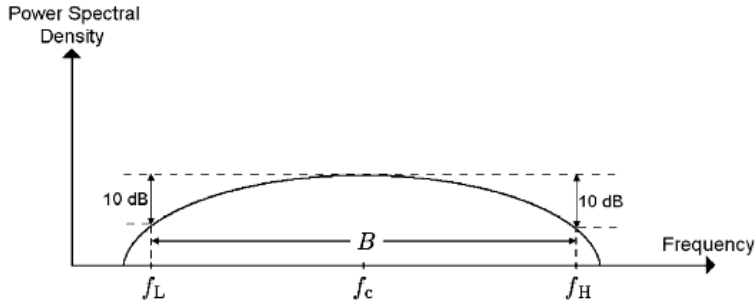


Figure 2. Definition of a UWB signal. Source [9]

Since the UWB systems are characterized by very large bandwidth, the UWB signal has very short waveform duration, usually in the order of nanoseconds due to the inverse relation between the bandwidth and the duration of a signal. The spread spectrum radio technologies based on CDMA typically use a few 100 times kilohertz to 10 times of megahertz of bandwidth. By contrast, the UWB signals are typically spread over a few gigahertz, which can be achieved by the repetition of transmitting an impulse-like waveform.

An example of an individual UWB pulse is shown in figure 3. As shown in figure 4, the ratio between the pulse duration (T) and the average time between neighboring transmissions (t) is often small. Such a pulse based UWB signaling scheme is called impulse radio (IR) UWB [10]. The position related parameters (parameters that can be used to localize the target) of the IR UWB signals such as its time of arrival (TOA) or time difference of arrival are the main focus in positioning systems [7].

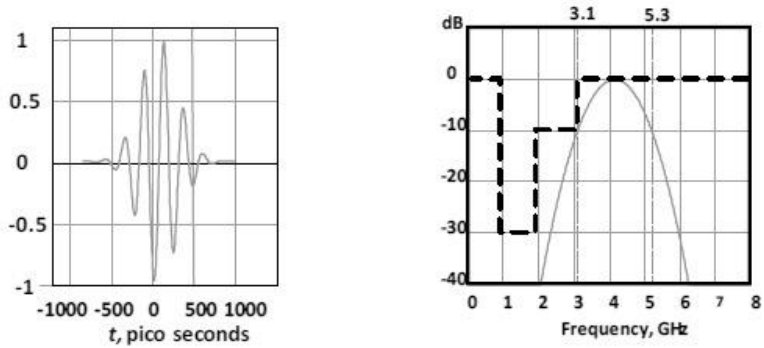


Figure 3. UWB waveform shown in time domain (left) and frequency domain (right) [13].

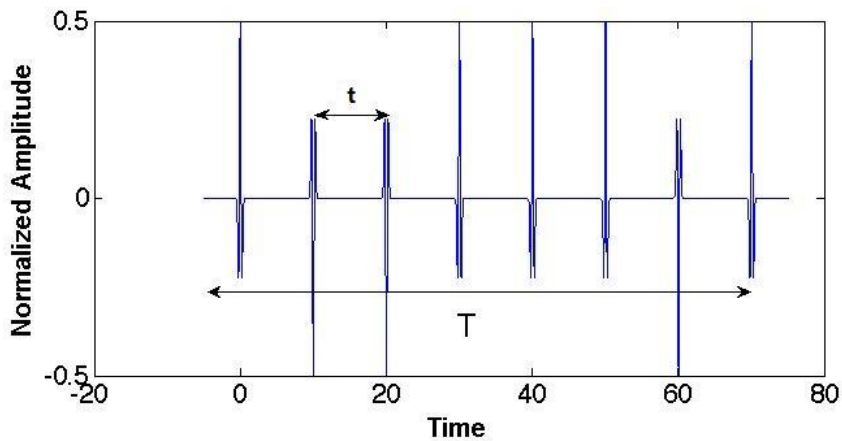


Figure 4. Example of a UWB signal with short duration pulses with a low duty cycle [7].

There are many advantages for positioning, communications, and radar applications because of the large bandwidths of UWB signals [9]:

- Accurate position estimation;
- Robust performance in multipath environment;
- Communications with very low RF profiles;
- Penetration through obstacles;
- High data rate transmission;
- Low cost and low power consumption.

As a result of the large spectrum that includes both low frequency and high frequency components, the UWB signal has the capability of penetrating object like walls, doors etc. Moreover, the high time resolution

provided by the large bandwidth could improve accuracy especially in indoor environment which typically have huge amounts of multipath component.

Especially, short-range wireless sensor networks (WSNs), which combine low/medium data-rate communications with positioning is an interesting application of UWB [7, 11]. Some important applications of UWB WSNs are [7, 9, 11, 12]:

- Security/Military: locating authorized people in high-security areas and tracking the positions of the military personnel;
- Medical: wireless body area networking for health and medical purposes;
- Search and Rescue: locating lost children, emergency responders, miners, and firemen.
- Inventory Control: real-time tracking of goods and valuable items in manufacturing plants, and locating precious equipment.
- Smart Homes: home security, control of home appliances.

The requirements of accuracy vary depending on the specific application in these positioning scenarios, But the possibility of achieving centimeter accuracy makes UWB signaling attractive in these scenarios [12].

1.2 PlusON410 Unit

In this thesis work, PlusON410 (P410) units have been used to generate and receive UWB signals. P410 is a versatile and agile UWB platform produced by Time Domain. Figure 5 shows a P410 Unit.



Figure 5. Photo of the P410 unit.

The P410 unit relies on low duty cycle transmission, with coherent signal processing and typical repetition rates of 10 Hz [13].

1.3 Position Estimation Schemes

Position estimation of a node in a wireless network need signal that exchanges between target node and several reference nodes [14]. If the target node can estimate the location by itself, it is called self-positioning. If the position of target node can be estimated by a central unit, which gathers position information from the reference nodes, it is called remote-positioning or network-centric positioning [15]. There are two basic approaches for positioning system: direct positioning and two-step positioning method. Direct positioning means that the position is estimated directly from the signals traveling between the nodes [16]. By contrast, the two-step positioning extracts certain signal parameters from the signals and then estimates positions according to these parameters. The latter one has significantly lower complexity than the direct one. Hence, the two-step approach is the common technique in most positioning systems [7], which also is the main focus of this thesis work.

Four main propagation parameters that can be used to derive the position estimates are: received signal strength (RSS), time-of-arrival (TOA), time difference of arrival (TDOA) and angle-of-arrival (AOA). Different techniques for the two-step positioning approach are describes in the following.

1.3.1 Received Signal Strength (RSS)

The received signal strength indicates the power of the received signal. Since the signal loses power with increasing travelling distance, the RSS is a distance based positioning parameter. As illustrated in figure 6, d_1 to d_3 is the distance from target to reference node, the position of the target node can be determined by using the well-known triangulation approach if the target node has the distance to at least three reference nodes [17]. A common model for path loss is given by [18]

$$\bar{P}(d) = P_0 - 10n_p \log(d/d_0). \quad (5)$$

where n_p is is the path-loss exponent, typically between two and four, $\bar{P}(d)$ is the average received power in decibels at a distance d , and P_0 is the received power at a short reference distance d_0 . Although formula (6) only indicates a simple relation between the received power and distance,

the exact relation between the signal power and distance in real environments is more complicated. Because of propagation mechanisms such as reflection, diffraction and scattering, the RSS will fluctuate even over a short distance. The signal power is commonly obtained by an averaging operation in order to mitigate the short-term fluctuating, which is called small scale fading. The average signal power can be calculated as follows [7]:

$$\bar{P}(d) = \frac{1}{T} \int_0^T |r(t, d)|^2 dt, \quad (6)$$

where $r(t, d)$ is the received signal at distance d and T is the integration interval. Although the average operation can mitigate the small-scale fading effects, the RSS measurements still have the environment-dependent errors because of shadowing, which is the attenuation of a signal due to passing through obstructions. Shadowing is commonly modeled by a zero-mean Gaussian random variable in logarithmic scale. Therefore the received power can be modeled as [7]

$$P(d) \sim \mathcal{N}(\bar{P}(d), \sigma_{sh}^2), \quad (7)$$

where σ_{sh}^2 is the variance of the zero mean Gaussian random variable representing the log-normal channel shadowing effect.

Equation (8) indicates that a reliable distance estimated from the RSS based measurement requires an accurate path-loss exponent and shadowing variance [11]. The accuracy of the estimation is given by the Cramer-Rao lower bound (CRLB) [19]:

$$\sqrt{\text{Var}(\hat{d})} \geq \frac{\ln 10}{10} \frac{\sigma_{sh}}{n_p} d, \quad (8)$$

where \hat{d} represents an unbiased estimate of the distance d , n_p is the path-loss exponent, and σ_{sh} is the standard deviation of shadowing. Observe from (8) that the range estimate will get more accurate as the standard deviation of the shadowing decreases, and get less accurate as the distance between the nodes increases.

RSS based positioning algorithms are very sensitive to the knowledge of the characteristics of the channel. It can't provide very accurate position estimates due to its high dependence on the channel parameters. The UWB

signal is not very useful to increase the accuracy in RSS based positioning systems [11].

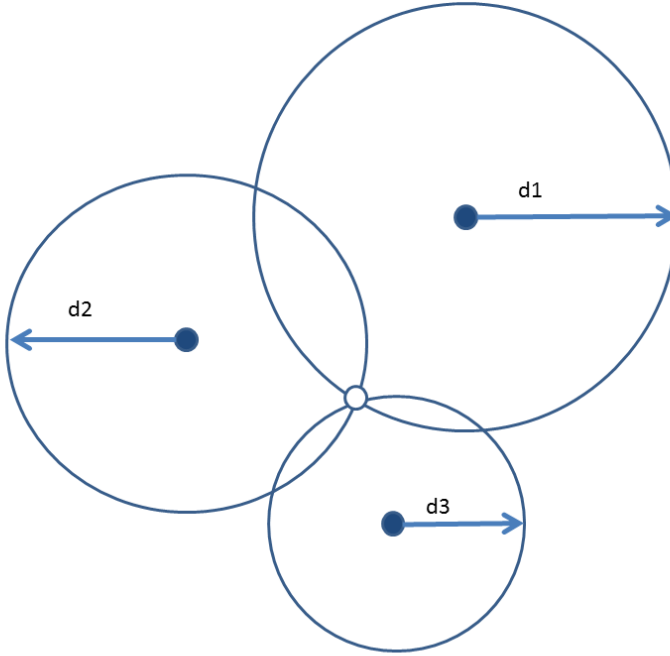


Figure 6. Distance-based positioning technique [7].

1.3.2 Time of arrival (TOA)

Another positioning parameter is the arrival time of the incoming signal from the reference node. If the nodes have a common clock or can exchange time information by certain protocols [20, 21], the TOA and the time when the signal is transmitted by the reference node can be used to calculate the distance between the target node and reference node since the propagation velocity (speed of light) is well known. The receiver's ability to accurately estimate the arrival time of the line-of-sight (LOS) signal is the foundation of time-based system.

A matched filter or a bank of correlation receivers are the optimal ways to estimate the arrival time [22]. In the former approach the arrival time is given by the instant when the filter output attains its peak, and the latter one estimates the arrival time by the time shift of the template signal that yields the largest cross correlation with the received signal [11]. The basic principle behind the correlation the receiver can be explained as

follows: $s(t)$ is transmitted from one node to another, the received signal is expressed as

$$r(t) = s(t - \tau) + n(t). \quad (9)$$

Where τ is the propagation delay and $n(t)$ is the background noise, which is commonly modeled as a zero-mean white Gaussian process. The correlation receiver correlates the received signal $r(t)$ with a local template $s(t - \hat{\tau})$ for various delays $\hat{\tau}$ and estimate the delay according to the correlation peak [7]:

$$\hat{\tau}_{TOA} = \arg \max_{\tau} \int r(t)s(t - \hat{\tau})dt. \quad (10)$$

From (9) and (10), the maximum correlation output is obtained at $\hat{\tau} = \tau$ in the absence of noise.

The matched filter receiver is mathematically equivalent to the correlation receiver. The correlation receiver requires a large number of correlators in parallel. The matched filter needs only one filter and also needs a device or a program that can identify the instant at which the filter output attains its large value. Therefore, the design and implementation costs will determine the specific receiver that will be used [11].

In realistic scenarios, the main source of errors for TOA-based systems is multipath propagation [11]. The multipath propagation creates a mismatch between the received signal of interest and the transmitted template used, which may shift the largest correlation output to incorrect timing. Hence, some high resolution time delay estimation techniques have been proposed in order to cancel the mismatch [23]. The employment of UWB signal can prevent this effect without the use of complex algorithms due to the large bandwidth. In addition, the first signal of arrival may not be the strongest signal in multipath channel, the first arriving signal detection algorithm has to be used to identify the correct one among the multiple correlation peaks [11].

The accuracy limit is given by the CRLB on the variance of the TOA estimate in a multipath-free channel. As

$$\sqrt{Var(\hat{\tau})} \geq \frac{1}{2\sqrt{2\pi}\sqrt{SNR}\beta}, \quad (11)$$

where $\hat{\tau}$ represents an TOA estimate, and β is the effective bandwidth [24, 25]. As demonstrated in (11), the increase of SNR and effective

bandwidth is beneficial to the accuracy. Consequently, the large bandwidth provided by UWB signals can offer very precise TOA measurements. Since travel time is determined by subtracting the known transmit time from the measured TOA, synchronization is required between the target node and the reference node. Hence, the resolution of the clock also affects the accuracy of the TOA measurement. However, in an asynchronous scenario, the travel time cannot be obtained since the receiver does not have knowledge about the transmit time. Then the two-way (or round-trip) TOA approach can be used. In this approach, the receiver will reply a signal after it receives a signal from the transmitter. Therefore, the time-delay for the transmitter is twice the propagation time to the receiver plus a reply interval (the time between receiver receive a signal and transmit a signal back) that is either known, or measured from the receiver [18].

1.3.3 Time difference of Arrival (TDOA)

Another time-based approach is based on the delay difference between the target node and two reference nodes, which is called time difference of arrival (TDOA). The delay difference can be estimated unambiguously if there is synchronization among the reference node [7, 17]. There are two approaches to obtain the TDOA. One way is to use TOA estimates related to the signals traveling between the target node and two reference nodes. The TDOA can be obtained from the TOA estimates since they have same timing offset due to the synchronization between the reference nodes [14].

Another way to obtain the TDOA is to perform cross-correlations of the two signals traveling between the target node and the reference nodes to calculate the delay corresponding to the largest cross-correlation value is [7, 26]. It can be described as:

$$\hat{\tau}_{\text{TDOA}} = \arg \max_{\tau} \left| \int_0^T r_1(t)r_2(t + \tau)dt \right|, \quad (12)$$

where $r_1(t)$ and $r_2(t)$ represent the signal traveling between the target node and the reference nodes and T is the observation interval [7].

In general, the TDOA scheme shares most of the advantages and drawbacks of the TOA scheme since they have many similarities. But there are some particular differences. Only synchronization on the reference nodes is needed, which is less expensive than synchronizing all the units in the TOA scheme [27]. Secondly, it needs to consume a measurement to

cancel out the clock bias. Hence, the TDOA system has worse accuracy than TOA system with the same system geometry [28].

1.3.4 Angle of arrival (AOA)

The last position related parameter is AOA, which is the angle from the different reference nodes. The intersections of direction information from several reference nodes give the position value [1].

The AOA information is commonly measured in two ways [18]. The most common way is estimate the AOA of the signal arriving at the node which employs multiple antennas in the form of an antenna array. The angle information for a known array geometry can be tracked from the difference in arrival times of an incoming signal at different antenna elements [14]. Figure 7 shows a uniform linear array (ULA) configuration. If there are sufficiently large distances between the transmitting and receiving nodes, the incoming signal arrives at consecutive array elements with $l \sin \alpha / c$ seconds difference, where l is the spacing between two array elements, α is the angle of arrival, and c represents the speed of light [7, 9].

Another approach for AOA estimation is to use the RSS ratio between two directional antennas pointed in different directions. The ratio of their individual RSS values can be used to estimate AOA since their main beams overlap [18].

The accuracy of AOA is also calculated from the lower bounds. The CRLB for the variance of AOA estimate $\hat{\alpha}$ for a ULA with N_a elements can be presented as follow when the signal arrives at each antenna element via a single path [29].

$$\sqrt{\text{Var}\{\hat{\alpha}\}} \geq \frac{\sqrt{3}c}{\sqrt{2\pi\sqrt{\text{SNR}}\beta\sqrt{N_a(N_a^2-1)}\ell\cos\alpha}}, \quad (13)$$

where α is the AOA, c is the speed of light, SNR is the signal-to-noise ratio for each element, which is assumed same for all antenna elements, ℓ is the spacing between elements, and β is the effective bandwidth [7]. The relation (12) implies that the increase of SNR, effective bandwidth, the total length of the array lead to increased accuracy.

UWB positioning systems perform badly for AOA scheme. As described above, both AOA estimates approached need multiple antenna elements, which can increase the sensor device cost and size. In contrast, one of the main advantages of a UWB system is the low-cost transceiver.

Another reason is time delay in a narrow-band signal can be approximately represented by a phase shift, the direction of signal arrival can be estimated from testing the combinations of the phase-shifted versions of received signals at array elements in various angles [17]. For pulse based UWB systems, a time delay cannot be represented by a unique phase value for a UWB signal, so the time-delayed versions of received signals should be considered [7]. Another reason is that the large bandwidth of UWB can resolve multipath components, especially in indoor environments. Accurate angle estimation will be very challenging in this situation [11].

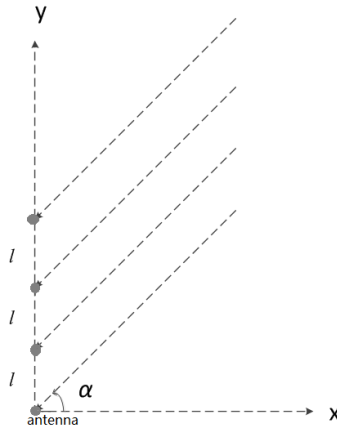


Figure 7. ULA configuration and a signal arriving at the ULA with an angle α [7].

1.4 Thesis aim

As described above, the large bandwidth of UWB signals provides high time resolution, thus time-based positioning system can which benefit from. As an example, the accuracy of an unbiased TOA range estimate using a pulse with 1 ns width is less than a centimeter at an SNR of 5 dB [7]. There is a critical limitation of the time-based positioning systems in synchronization. Synchronization between the target node and the reference nodes, or synchronization between reference nodes, is needed. In this thesis, the authors try to develop a method to localize nodes in the unsynchronized scenario, and to verify it in realistic environment. It involves UWB signal positioning using an unsynchronized time of arrival (UTOA) algorithm that is implemented to sensor network formed by several P410 units. The thesis work is divided into two phases:

- 1) Design and develop method to allow all units communicate with each other in proper time slots and make the network self-organized;

-
- 2) Implement the algorithm in a realistic environment, and analyze data from the measurements.

1.5 Thesis outline

This thesis is structured as follows:

- Chapter 2 provides the principle of unsynchronized time of arrival (UTOA), verification of the P410 units' configuration and an outdoor pre-test,
- Chapter 3 covers three different multi-unit measurements, non-far field 2D case, 2D case and the 2D far field case;
- Chapter 4 describes the far field unsynchronized time of arrival (FFUTOA) algorithm and provides some results;
- Chapter 5 discusses the 2D/3D far field case;
- Chapter 6 concludes the thesis work, and suggests future improvements.

CHAPTER 2

2 Pre-test and verification

In this chapter, the principle of the UTOA, P410 units' configurations and a pre-test scenario condition in which measurements were conducted are described. The pre-tests provide fundamental results for later test and verifications in Chapter 3.

2.1 Principle of the UTOA

As mentioned above, the main purpose is to apply a time-based algorithm using UWB signal to estimate positions in an unsynchronized scenario, and to verify the algorithm in realistic environments. In the ideal setup for the network formed by several sensors, the sensor can be either transmitter or receiver. The sensor can be transmitter and transmit UWB signals when it sense that the medium is free, the rest of the sensors will receive this UWB signal and record the time when they received it. There will be a different time of arrival between the different sensors since the sensors are located at different positions. The sensor which transmitted this signal will then turn back to receiver again. Then remaining sensors will sense the media again and repeat the step stated above. After multiplication with the speed of light c , each time of arrival corresponds to a different distance between the transmitter and receiver such that $d_{i,j} = c\tau_{ij}$, where the $d_{i,j}$ represents the distance difference, τ_{ij} is the time of arrival. Then the problem becomes to for given measurements of $d_{i,j}$, determine both transmitter positions and receiver positions [30].

Assume that $r_i, i = 1, \dots, m$ and $t_j, j = 1, \dots, k$ are the spatial coordinates of m receivers and k transmitters, respectively. Because of neither receivers or transmitters are synchronized, we have

$$\delta_{i,j} = |r_i - t_j| + f_i + \tilde{g}_j, \quad (15)$$

where f_i, \tilde{g}_j are the unknown offsets for receivers and transmitters, respectively.

Furthermore, if the transmitters are so far from the receivers that a transmitter can be considered to have a common direction to the receivers, we have

$$\delta_{i,j} = |r_i - t_j| + f_i + \tilde{g}_j \approx |r_i - t_j| + (r_i - r_1)^T n_j + f_i + \tilde{g}_j = r_i^T n_j + \bar{g}_j + f_i + \tilde{g}_j, \quad (16)$$

where $\bar{g}_j = |r_1 - t_j| - r_1^T n_j$ and n_j is the direction of unit length from transmitter j to the receivers. The far field approximation can be obtained by setting $g_j = \bar{g}_j + \tilde{g}_j$ [31].

$$\delta_{i,j} = r_i^T n_j + f_i + g_j. \quad (17)$$

The positions can be determined from [30]

$$\arg_{r_i, t_j, n_j, |n_j|=1} \min \sum_{i,j} |d_{i,j} - (r_i^T n_j + f_i + g_j)|^2. \quad (18)$$

The starting point for (18) is obtained by applying the algorithm below [30]:

1. Set $\bar{D}_{i,j} = D_{i,j} - D_{1,j}$, where the $D_{i,j}$ is the collection of $d_{i,j}$;
2. Remove first row of \bar{D} ;
3. Calculate the singular value decomposition (SVD) $\bar{D} = USV^T$;
4. Set \tilde{R} to the first 3 columns of U and \tilde{N} to first 3 columns of SV^T ;
5. Solve for the unknowns in the symmetric matrix B using $\tilde{n}_j^T B \tilde{n}_j = 1$;
6. Use Cholesky factorization of B calculate A : $B = AA^T$;
7. Transform motion according to $R = (\tilde{R}A^{-1})^T$ and structure according to $N = A\tilde{N}$.

The algorithm above requires a far field assumption, which approximately means that the transmitter receiver distances are more than four times larger than inter-receiver distances.

The non-far field 2D case selects the some Gauss variables randomly as starting point.

Once the initial estimate has been found, it is straightforward to extend the solution to all positions of receivers and transmitters.

The ideal setup stated above requires a low level programming of the sensors, which is hard to perform with the P410 units. Therefore, some adaptations are required to design the setup. As illustrated in figure 9, only one stationary transmitter, m receivers (r_i) and k dynamic scatters (s_j) are present. Dynamic scatter means that there is only one scatter each time slot, but it will move to another position in next time slot, and it has j positions in total. The transmitter will continue transmitting UWB signals, and the time of arrival for received signal from LOS path and scattered paths will recorded by the receiver. After the dynamic scatter has moved to all j positions, the data recorded by the receiver will be analyzed on a computer.

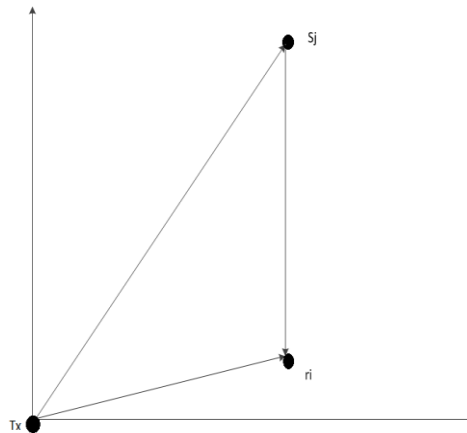


Figure 8. The sketch for adapted design.

In this scenario, the scatters can be treated as virtual transmitters compared to the functionality of the transmitter in ideal case. The only difference is there will be a stationary parameter in each f_i , which denotes the distance between the static transmitter to receivers. The figure of complete setup design can be found in Chapter 3.

In order to obtain the $d_{i,j}$ in the realistic environments, several measurements has been made.

2.2 P410 configuration

Two kinds of configurations for P410 units are considered in the test: at the transmit side and at the receive side. Before starting the TX or RXs, several factors need to be introduced and set up.

2.2.1 Transmit configuration

1) Transmit signal

Figure 9 shows the normalized transmit signal with a length of 6 ns generated by the P410 unit transmitter. The transmit signal has a high resolution scale [32].

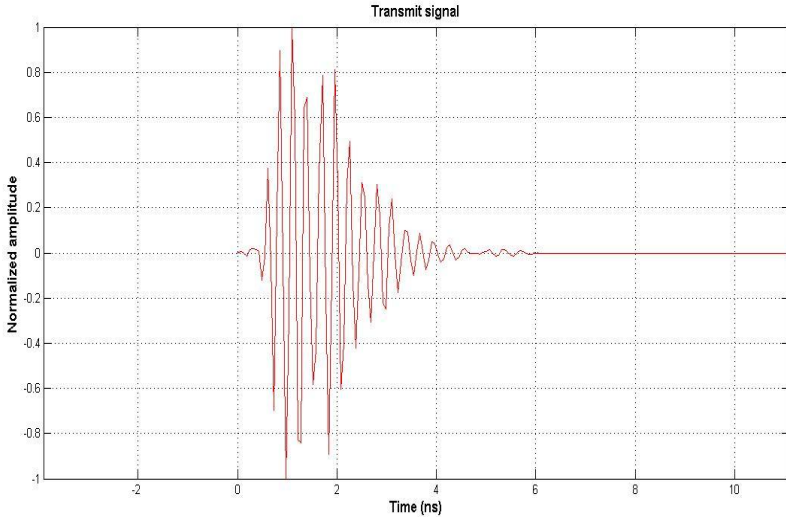


Figure 9. Transmit signal.

2) Packet to send

The concept of packet in this thesis work is defined as a data set, which contains 1632 samples. Each sample is 61.035 ps. The “packets to send” declares the number of packets that will be sent during the test.

3) Transmit gain versus transmit power

The following table shows the relationship between the transmit gain and the transmit power delivered to antenna port for the P410 unit. The default transmit gain is 44 which corresponds to -14.5 dBm transmit power [32]. The largest transmit gain is 63.

Table 1. Relationship between TX gain and TX power for P410 units [33].

Transmit gain	Transmit power (dBm)
63	-12.64
59	-12.88
55	-13.2
51	-13.62
47	-14.12

43	-14.78
39	-15.57
35	-16.47
31	-17.43
27	-18.61
23	-20.0
19	-21.6
15	-23.32
11	-25.35
7	-27.58
3	-29.89
0	-31.6

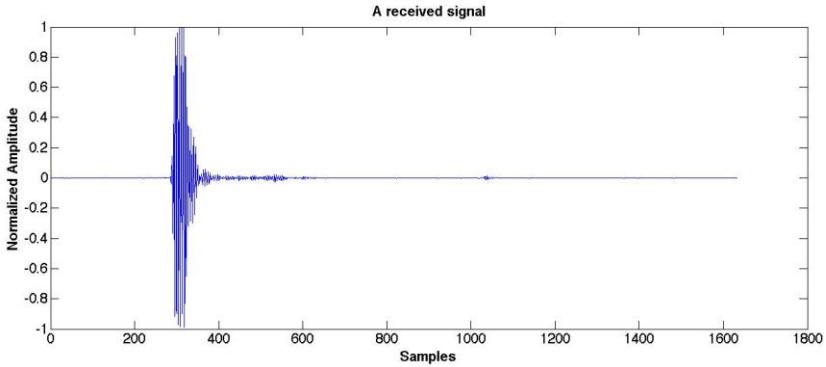
4) Acquisition Pulse Integration Index (Acquisition PII)

The pulse integration index (PII) is an important factor, which is useful for increasing the operation range, minimizing error, and capturing high SNR waveforms. For example, pulse integration 2^6 , corresponds to a PII of 6 and Acquisition PII of 7. It corresponds to double the pulse integration, which is from 64:1 to 128:1. Thus, the SNR of the received signal will be improved by 3dB. Acquisition PII default value is 7. The largest value of Acquisition PII is 11 [33].

2.2.2 Receive configuration

1) Receive signal

Figure 10 shows an example of one receive packet. Figure 11 is the received LOS component. The amplitude is normalized in both figures. Due to the high-resolution characteristic, the multipath components could be observed around sample number 300, and around sample number 1050.



10. A received packet.

The transmit signal last 6 ns, which equals around 100 samples with a sample length of 61.035ps. The LOS component is clear to observe in figure 11, thus the TOA of LOS path can be acquired precisely. The 3rd, 4th, 5th lobes in figure 11 indicate the overlap from multipath components compare the transmit signal in figure 9 to the received LOS signal in figure 11.

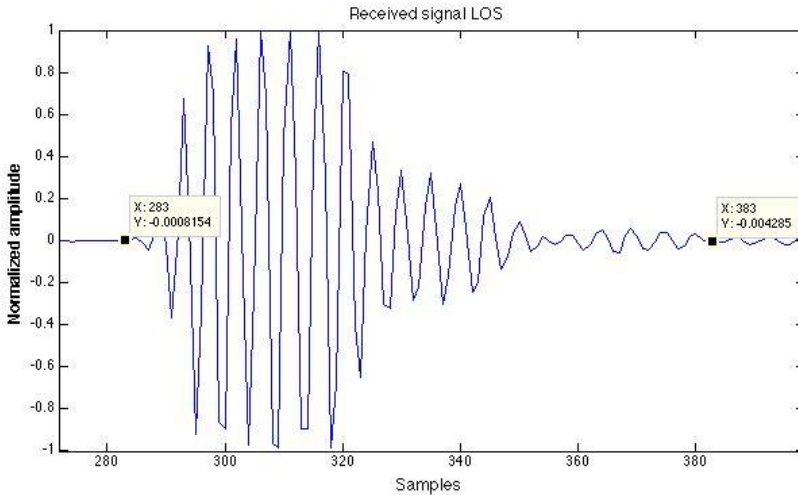


Figure 11. Received signal | LOS.

Figure 12 is an example of a 50-packet receive signal. LOS components are aligned. Six obvious scatter components can be observed from 50 to 80 ns. The scatter components are named S1 to S6 separately.

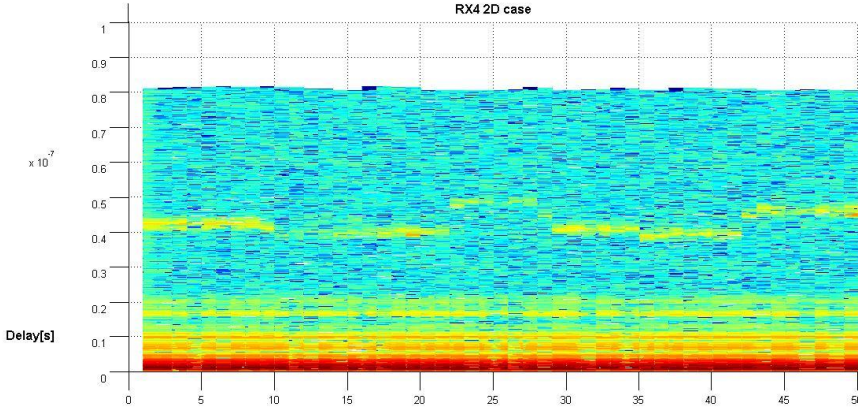


Figure 12. Received signal, 50 packets.

2) Different distance (D_d)

The distance between the LOS component and scattered path components are defined as D_d . The D_d_signal is defined as the distance processed from data for instance from figure12. The algorithm to calculate D_d_signal is as follows:

- i) Align all the LOS components.
- ii) Find the start time of scatter for each packet.
- iii) Estimate the number of packets that represent the certain scatterer.

Take receive signals in figure 12 as an example, packets from number 1 to 9 represent reflected signals from S1; packets from 10 to 21 represent reflected signals from S2, however, the amplitude of packet number 10 to 15 are weak, thus for S2, packet number 16 to 21 are taken into consideration other than 10 to 21; for S3, reflected signals of packet number 22 to 27 are used; for S4, signals of packet number 28 to 33 are clear and relatively strong, they are used for the later calculation; for S5 and S6, the used packet number are 34 to 41 and 42 to 50 respectively.

- iv) Average the start time for S1 to S6 separately.
- v) D_d_signal of S1 to S6 equals the product of average start time for each scatter and the speed of light.

In order to have better receive signal SNR, two factors need to be considered, one is transmit gain/transmit power and the other is Acquisition PII. For a maximized SNR, transmit gain is set as 63, Acquisition PII as 11. Table 2 shows the configuration for the outdoor pre-test, where the transmit gain is 63, transmit power is -12.64 dBm, packet to send is 50 and the Acquisition PII is 11.

Table 2. TX configuration for the outdoor pre-test.

TX configuration	Transmit Gain	Transmit Power	Packet to Send	Acquisition PII
Outdoor pre-test	63	-12.64 dBm	50	11

2.3 Outdoor Pre-test

The outdoor test is performed in an open place in Lund, Sweden showed in figure 13. The red oval in the map marks the specific location. The place is considered suitable because it is an area with few reflectors and moving scatters.

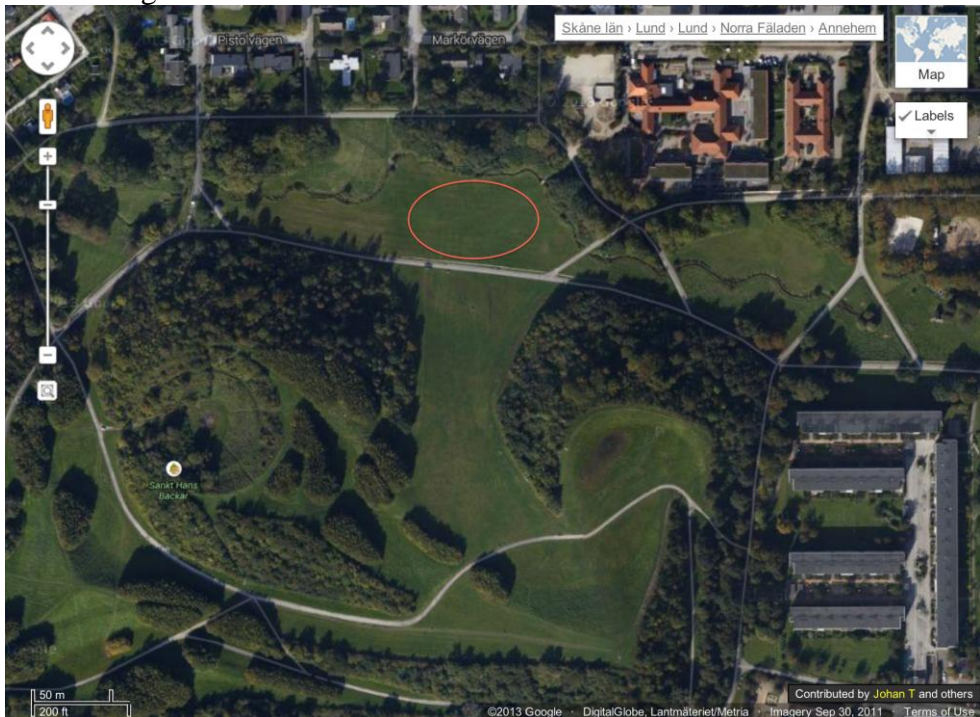


Figure 13. Outdoor test scenario in map.

Figure 14 shows the setup of the measurement while table 3 shows the dimensions. The scatterer used for the measurement is a pipe, which is shown in figure 15. The pipe is 75 cm long, with a diameter of 10 cm.

It takes around 200 seconds to send all 50 packets. In the first 20 and the last 20 seconds, the pipe remains static. During other times, for the first time the pipe moves with a uniform speed from the start position to the end position, while for the second time, the pipe moves with a uniform speed from end position to the start position.

The start position and end position are denoted as Start and End in table 3.

In this report, only the data received by RX2 are analyzed. The two results are shown in figure 16 and 17.

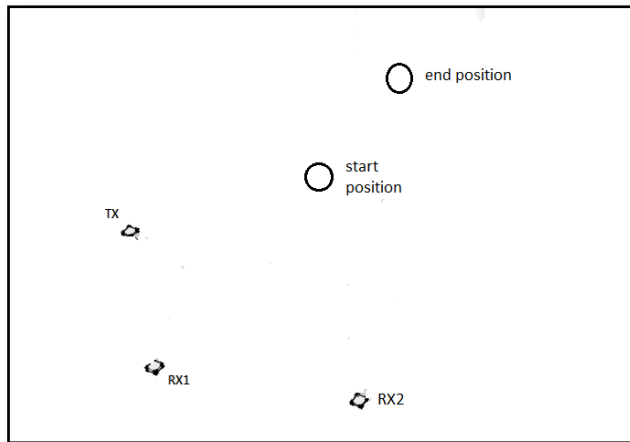


Figure 14. Outdoor pre-test setup.



Figure 15. Pipe as scatterer.

Table 3. Scales of RX2 | Start to End& End to Start.

	TX-RX2	TX-Start	RX2-Start	TX-End	RX2-End
scales	6.425 m	4.032m	4.610m	6.527 m	8.264m

In figure 16 and 17, obvious scatter components indicating the uniformly-speed moving scatter are observed.

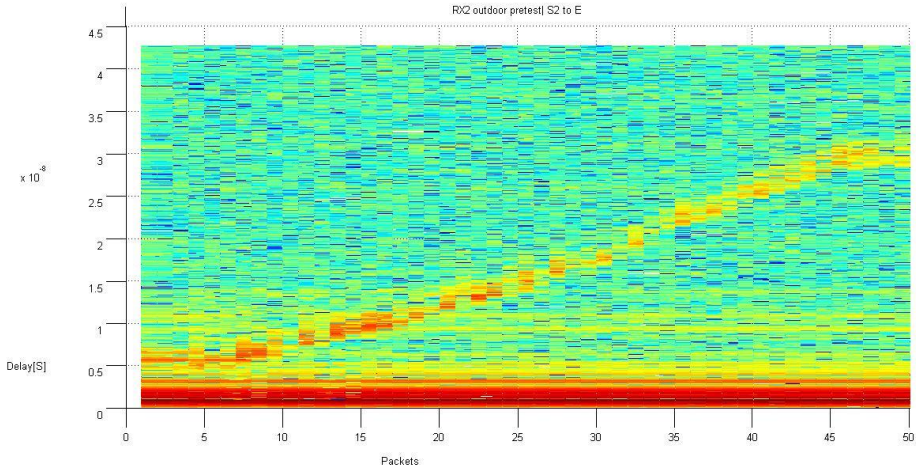


Figure 16. RX2 outdoor pre-test | Start to End.

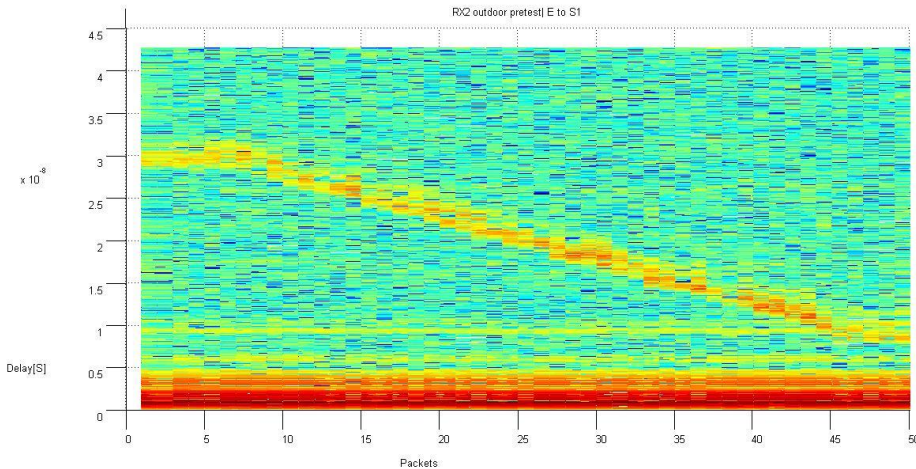


Figure 17. RX2 outdoor pre-test | End to Start.

Table 4 shows that the outdoor pre-test provided a good result with accuracy of 5 or 7 cm and 0.235 or 0.19 ns. It proves that the P410 units not only work fine in the outdoor scenario but with a high resolution.

Table 4. Comparison of delay for position Start and End between scale and P410 test for RX2.

	Scale	P410 test	Difference	Accuracy
Start	7.39 ns	7.625 ns	0.235 ns	0.0705 m
End	27.88 ns	27.69 ns	0.19 ns	0.057 m

2.4 Conclusion

This pre-test succeeds in two ways. Firstly, the scatterer can be observed easily from the received signals in figure 16 and figure 17, which indicate a good receiving SNR. Secondly, the accuracy shown in table 4 is in ns, which is a very high resolution with the practical test environment.

A high receive SNR means the TX configuration in table 2 is proven to be sufficiently enough, as well as that using pipe as scatterer provide strong enough reflection. It proves that the specific open field is a suitable place for further testing. There is no obvious interference. The pre-test provides fundamental possibility for the later test as well as for the UTOA and FFUTOA algorithm to be used.

CHAPTER 3

3 Multi-unit measurement

In this chapter, descriptions of non-far field 2D, 2D and 2D far field case are provided. For all three cases, 7 units are used. Unit ID 100 is used as TX, 101 as RX1, 102 as RX2, 103 as RX3, 104 as RX4, 105 as RX5, and 107 as RX6. The pipe in figure 15 is used as scatterer and it moves to 9 positions. Same as the pre-test, the transmit gain is set as 63 and the Acquisition PII is 11.

In the non-far field 2D case, a coordinate system is made using a ruler. Positions of the TX, RXs and Scatterers are pre-determined; distances between the TX, RXs and Scatterers are calculated from the dimensions. Distances between units are recorded by a range request application [33] carried by the P410 units as well. Data and receive signals are given in Appendix 1.

Instead of a coordinate system, two reference points (Ref1/Ref2) are used for measuring distances in the 2D and the 2D far field cases. Distances between TX/RXs/Scatterers and Ref1/Ref2, RXs and TX, TX and Scatterers, Scatterers and RXs are measured by the ruler as well as a laser meter. The distances and receive signals of 2D case are given in Appendix 2, while distances and receive signals of the 2D far field case are recorded in Appendix 3.

Processing of measurement data requires three steps. The first step is to get the ground truth information, which is position of TX, RXs and Scatterers. Second step is to process receive signal of all packets, set packet as x-axis, delay time as y-axis, and amplitude in dB as z-axis. The last step is to get D_d_signal from receive signals using algorithm described in Chapter 2.

3.1 non-far field 2D case

Figure 18 shows the coordinate system that is made for the non-far field case. As shown in figure 18, the TX is located in the middle RXs and Scatterers are located randomly.

Positions of TX, RXs and Scatterers are given in table 5, 6 and 7.

Positions designated in figure 18 are represented as *Designated*, while positions calculated from measured data in practical situations by range requests in Appendix 1 are represented as *Measured* in the following tables. The first element in each position is the x-axis component, while the second is the y-axis component.

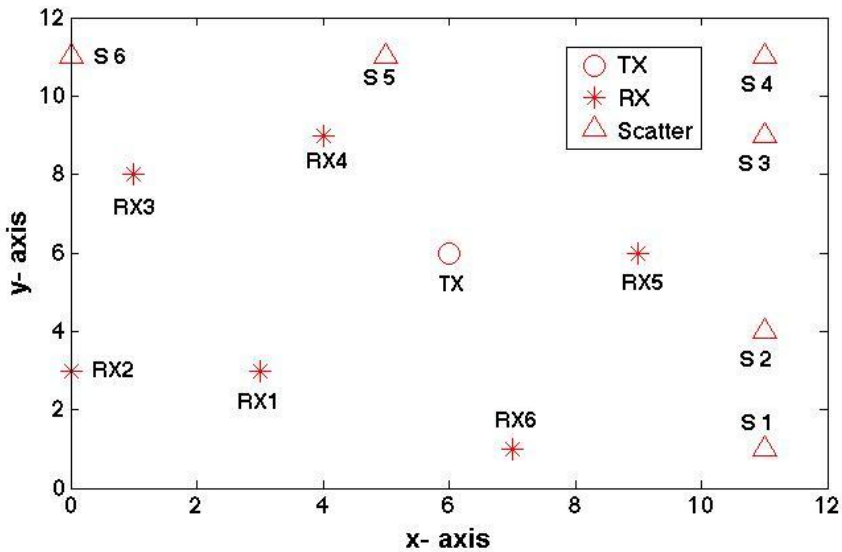


Figure 18. Positions of TX, RXs and Scatterers in the coordinate system.

Table 5. The TX position | non-far field 2D case (meters).

	TX
Designated	(6 6)
Measured	(6.021 6.286)

Table 6. The RXs positions | non-far field 2D case (meters).

	RX1	RX2	RX3	RX4	RX5	RX6
Designated	(3 3)	(0 3)	(1 8)	(4 9)	(9 6)	(7 1)
Measured	(3.078 2.952)	(-0.056 2.923)	(1.057 8.08)	(3.946 8.976)	(8.954 5.937)	(7 1)

Table 7. The Scatterers positions | non-far field 2D case (meters).

	S1	S2	S3	S4	S5	S6
Designated	(11 1)	(11 4)	(11 9)	(11 11)	(5 11)	(0 11)
Measured	(11 1)	(10.96 4.089)	(10.97 8.976)	(10.81 11.02)	(5.239 11.07)	(-0.423 10.5)

The non-far field 2D test is carried out as follows. TX transmits the signal and all six receivers receive at the same time, while the scatterer moves from scatterer 1 to scatterer 6. The LOS receive signals are signal transmitted from TX directly to RX1, RX2, RX3, RX4, RX5 and RX6. LOS components of the receive signals are aligned in figure 19 as well as in figures in Appendix 1. Signals reflected by the pipe and received by RX1, RX2, RX3, RX4, RX5 and RX6 are recorded as well as seen in figure 19.

The total time of the non-far field 2D test is 150 seconds. Altogether 50 packets are sent. Each scatterer position last 30s, which corresponds to around 4 packets.

In the Appendix 1, there lists receive signals of RX1 to RX6 are given, it could be observed that 1) the LOS components are quite obvious, and the are present amplitude of them varies around 50 dB; 2) two stable scatters located around 10 ns to 20 ns, the stable scatters have a high possibility to be computer screens in practical test environment; 3) six scatterer positions located around 30 ns to 60 ns are observed, and the amplitude of the reflected receive signals in dB are around 30 dB to 40 dB.

Figure 19 is an example of a non-far field 2D case receive signal, it shows the receive signals of RX1. Six scatterer positions are clearly observed, as well as stable scatters, which are around 20 ns and 30 ns. RX1 is used as analysis example for the non-far field 2D case, analyses for other receivers are similar.

Similar to D_d defined and explained in Chapter 2, D_d of the non-far field case is calculated for each scatter position for every receiver. $D_d_designated$ in the coordinate system by ruler, $D_d_measured$ recorded by P410 units, and D_d_signal that is calculated from receive signal. The time the signal travels from TX directly to each receiver is the time of LOS. By adding the distance of TX to scatterers and RX to scatterers, the distance of the signal travel to scatterers and reflect to receiver is calculated, thus the travel time is known. The subtracted time could be viewed as the travel time between zero and the time of scatter, which corresponding to the subtracted distance.

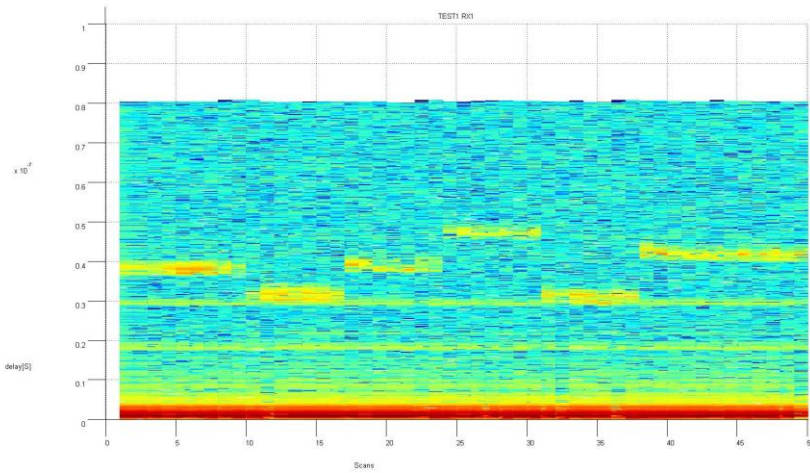


Figure 19. Receive signals of RX1 | non-far field 2D case.

In total, for RX1, referring to the measured data in Appendix 1, the $D_d_designed$ and $D_d_measured$ could be estimated, as showed in table 8. The D_d_signal of RX1 in table 8 represents the different distance processed by the D_d algorithm described in Chapter 2. D_d of RX2 to RX6 are listed in Appendix 1.

Table 8 shows that the processed data is quite accurate, which is a good result. The information got from the receive signal is reliable. The UTOA algorithm could be implemented based on the data.

Table 8. Dd (meter) for RX1 | non-far field 2D case (meters).

For RX1	Dd_designated	Dd_measured	Dd_signal
S1	11.074	10.871	10.943
S2	9.204	9.023	8.944
S3	11.588	11.135	11.187
S4	11.142	13.561	13.665
S5	9.102	8.705	8.884
S6	12.116	11.959	12.297

3.2 2D case

Figure 20 shows the scenario for 2D. TX is located in the middle of the RXs, RXs are around TX, and Scatterers are located around TX as a semicircle shape. Distances of TX to RXs are around 2.14 to 3.32 meter, distances of TX to Scatterers are around 7.39 to 9.53 meter, while distances of RX to Scatterers are around 4.81 to 12.48 meter, and detailed dimensions of figure 20 are listed in Appendix 2. Compared to the non-far field case, two reference points and laser meter are used for the measurement instead of using the coordinate system, the changes reduce the complication of the setup.

In the 2D case scenario, the receivers keep receiving and recording the signal when the transmitter keeps sending the signal and the scatterer moves from scatterer 1 to scatterer 6 every 50 seconds. The test takes in total 300 seconds, 60 packets are sent during this time. The transmit gain is set to 63 and Acquisition PII as 11.

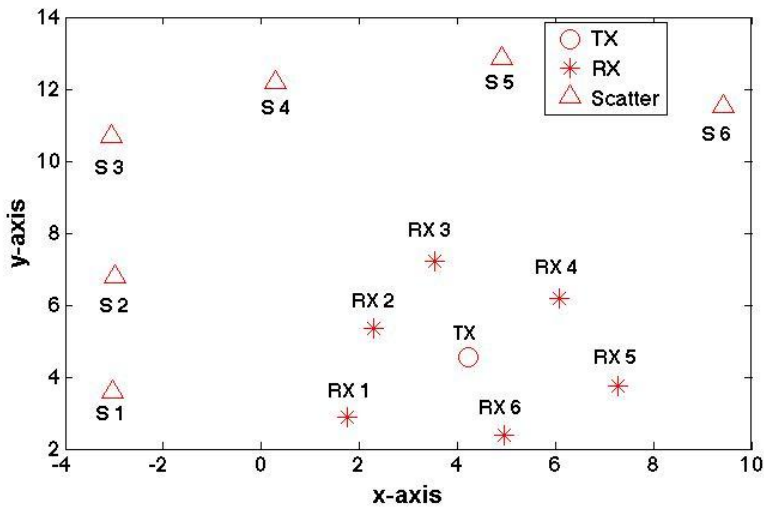


Figure 20. 2D case scenario.

For the later comparison in Chapter 4, the measured distances noted in Appendix 2 are transformed into positions. Distance between Ref1 to Ref2 measured by the ruler is 11 m, by laser meter is 11.115 m. Ref1 is set as (0,0) in the coordinate system, and Ref2 becomes (11, 0) by the ruler, and (11.115, 0) by the laser meter. Using two reference points, the distance between reference points and TX/RXs/Scatterers, and dimensions indicated in the figure 20 for calculations, results are filled into the following tables, table 9, 10 and 11. The first element in each position is the x-axis

component, while the second element is the y-axis component.

Table 9. The TX position | 2D case (meters).

	TX	
Ruler	(4.215	4.587)
Laser meter	(4.216	4.561)

Table 10. The RXs positions | 2D case (meters).

	RX1	RX2	RX3	RX4	RX5	RX6
Ruler	(4.96	(1.769	(2.333	(3.551	(6.097	(7.316
	2.413)	2.915)	5.397)	7.257)	6.220)	3.811)
Laser	(4.94	(1.751	(2.299	(3.528	(6.071	(7.273
meter	2.387)	2.872)	5.333)	7.204)	6.170)	3.761)

Table 11. The Scatterers positions | 2D case.

	S1	S2	S3	S4	S5	S6
Ruler	(-2.991	(-3.001	(-3.093	(0.34	(4.900	(9.411
	3.650)	6.763)	10.691)	12.25)	12.901)	11.551)
Laser	(-3.030	-2.983	(-3.064	(0.290	(4.891	(9.416
meter	3.577)	6.775)	10.687)	12.192)	12.854)	11.525)

From the receive signals of RX1 to RX6 listed in the Appendix 2, it could be observed that 1) the LOS component are quite obvious, and the amplitude of them in dB varies from 50 dB to 54 dB; 2) several stable scatters locate around 7 ns to 20 ns, the stable scatters have a high possibility to computer screens; 3) the six scatter positions located around 30 ns to 70 ns are easy to observe, the amplitude of the reflected signals in dB are around 25 dB to 30 dB.

Figure 21 is the received signal for RX4. In the rest of the 2D case analysis, RX4 is used as an example. The analysis for other receivers is similar to the RX4. Same as the D_d defined and explained in Chapter 2, D_d in this chapter is calculated for each scatterer position for every receiver. There are three kinds of D_d for the 2D case, the first one is the D_d_ruler is measured by ruler, the next one is the $D_d_laser\ meter$ is measured by laser meter and the last one is D_d_signal from receive signals. LOS components are aligned in figure 21. By adding the distance of TX to scatterers and RX to scatterers, the distance of the signal send to scatterers and reflect to receiver is calculated, thus the travel time is known. The subtracted time could be viewed as the time between zero and the time that the scatter component appears, for example in the figure 21.

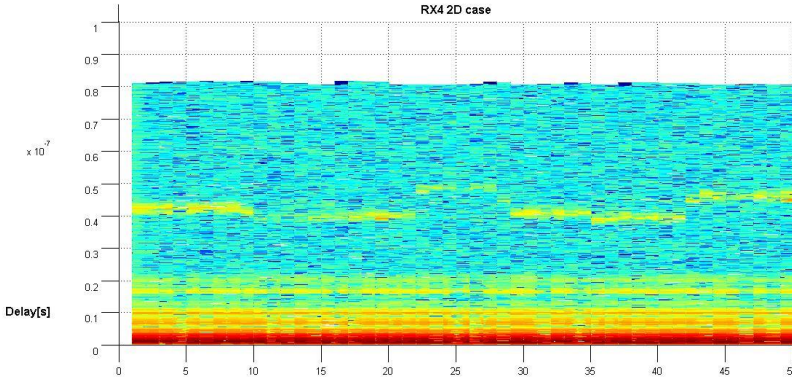


Figure 21. Receive signals of RX4 | 2D case.

All in all, for RX4, the D_d_ruler and $D_d_laser\ meter$ could be estimated, as showed in table 12. D_d_ruler , $D_d_laser\ meter$ and D_d_signal for the other five receivers are processed and recorded in Appendix 2.

Table 12 that shows comparisons of D_d , shows that the data processed is quite precise compare to ground truth measurements. The information processed from the receive signal is reliable.

Table 12. The difference distance for RX4 | 2D case (meters).

For RX4	Dd_ruler	Dd_laser	Dd_signal
S1	12,22	12,189	12.174
S2	11,46	11,409	11.455
S3	14,23	14,181	14.333
S4	11,7	11,647	11.689
S5	11,31	11,278	11.483
S6	13,23	13,247	13.363

3.3 2D far field case

Compared to the non-far field 2D case and 2D test, the 2D far field case has the following differences 1) RXs are roughly, placed within a circle, with radius 1.5 m; 2) instead of using 6 scatterers, 9 are used; 3) scatterers are placed in all directions.

Distances between TX and RXs are around 1.5 meter, distances between TX and Scatterers are around 8 to 12 meters, while distances

between RX and Scatterers are around approximately 8 to 13 meters, as shown in Appendix 3.

Figure 22 shows the setup for the 2D far field, detailed dimensions are reported in Appendix 3.

The test last for 600 seconds, and there are 9 scatterer positions, Scatterer 1 and Scatterer 9 occupy 90 seconds, and other scatterers occupy 60 seconds. During 600 seconds, 100 packets are sent. The transmit gain is set as 63 and Acquisition PII as 11.

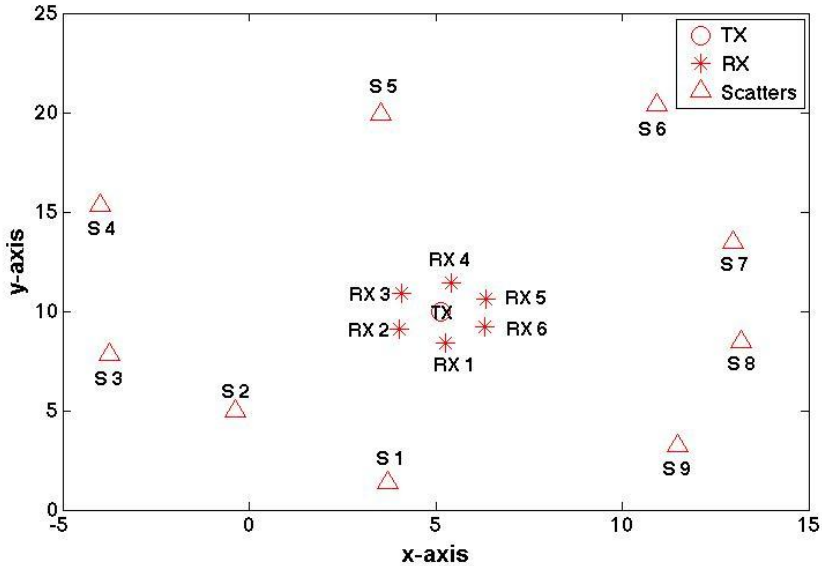


Figure 22. Test setup | 2D far field case (meters).

In order for later comparisons in Chapter 4, measured distances noted in Appendix 3 are converted into positions. Distance between Ref1 to Ref2 measured by the ruler is 10.85 m, by the laser meter is 10.966 m. We set Ref1 as (0,0) in the coordinate system, and Ref2 becomes (10.85, 0) by the ruler, and (10.966, 0) by the laser meter. Similar to the 2D case, using two reference points, the distance between reference points and TX/RXs/Scatterers, and setups indicated in the figure 22 for calculations, the results are filled into the following tables, table 13, 14 and 15. The first element in each position is the x-axis component, while the second element is the y-axis component.

Table 13. The TX position| 2D far field case (meters).

	TX	
Ruler	(5.143	9.938)
Laser meter	(5.130	9.960)

Table 14. The RXs positions| 2D far field case (meters).

	RX1	RX2	RX3	RX4	RX5	RX6
Ruler	(5.277 8.399)	(4.031 9.085)	(4.094 10.895)	(5.431 11.419)	(6.351 10.627)	(6.313 9.203)
Laser	(5.271 8.404)	(4.020 9.092)	(4.079 10.895)	(5.418 11.423)	(6.341 10.600)	(6.307 9.198)

Table 15. The Scatterers positions| 2D far field case (meters).

	S1	S2	S3	S4	S5	S6	S7	S8	S9
Ruler	(3.750 1.448)	(-0.350 4.938)	(-3.733 7.803)	(-4.072 15.297)	(3.593 19.908)	(11.179 20.317)	(12.986 13.441)	(13.212 8.425)	(11.478 3.178)
Laser meter	(3.717 1.393)	(-0.365 4.962)	(-3.742 7.834)	(-4.007 15.326)	(3.518 19.918)	(10.922 20.355)	(12.958 13.452)	(13.193 8.436)	(11.488 3.220)

From receive signals of RX1 to RX6 listed in the Appendix 3, it could be observed that 1) the LOS component is quite obvious, and the amplitude of it varies around 50 dB to 55 dB; 2) there are several stable scatterers locate around 10 ns, the stable scatterers have high possibility to be computer screens; 3) the nine scatterer positions locate around 40 ns to 80 ns are easy to be observe, the amplitude of the reflected receive signals in dB are around 30 dB to 40 dB; 4) scatterer number 6 is not possible to observe clearly in all receive signals, the received power is quite weak, thus scatterer 6 is ignored in the analysis.

Figure 23 shows the receive signal for RX1. RX1 is used as an example for the 2D far field case analysis. The analysis for other receivers is similar to the RX1. The LOS components are aligned for RX1. There are eight obvious scatterer positions.

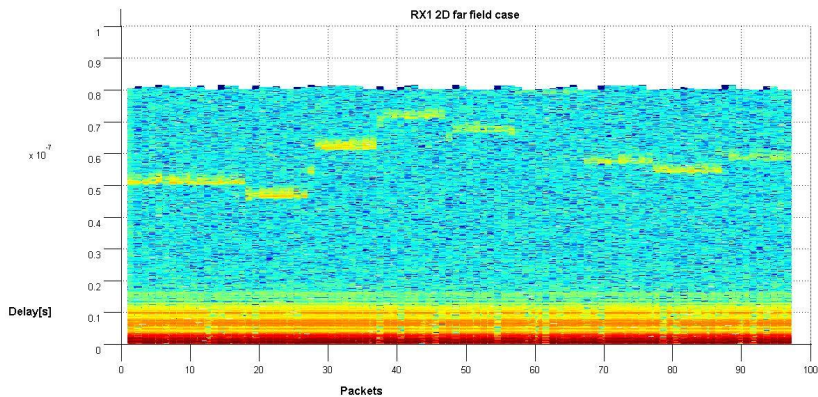


Figure 23. RX1 2D far field case.

Same as the D_d defined and explained in Chapter 2, D_d in this part is calculated for every scatterer position for each receiver. For RX1, the D_d_ruler and $D_d_laser\ meter$ are calculated. The D_d_signal of RX1 represents the different distance processed by the D_d algorithm in Chapter 2. Three kinds of D_d are recorded in the table 16. D_d_ruler , $D_d_laser\ meter$ and D_d_signal for the other five receivers are processed and recorded in Appendix 3.

Table 16. Difference distance for RX1 (meters).

For RX1	Dd_ruler	Dd_laser	Dd_signal
S1	15,05	15,028	14.992
S2	13,73	13,768	13.777
S3	18,32	18,335	18.328
S4	21,33	21,27	21.228
S5	19,99	19,944	19.994
S6	23,68	23,59	None
S7	16,99	16,967	16.977
S8	16,13	16,108	16.117
S9	17,37	17,361	17.469

As a summary, the data processed is good, and the information from the receive signal is reliable. The algorithm in [31] can be used with good results.

CHAPTER 4

4 Position estimates

This chapter describes comparisons between measured positions and the positions processed from algorithms described in Chapter 2. The estimates for the three cases described in Chapter 3 are listed.

4.1 Position estimates of the non-far field 2D case

The D matrix in table 17 gives the D_d_signal in meter for all the RXs, which are used to reconstructed positions of TX, RXs and Scatterers. Reconstructed positions are processed by algorithm in Chapter 2. Non- far field 2D case position estimates could be completed using a random s_j and r_i value to start with. In most of the simulations, results obtained could not make sense, estimates like in figure 24 could be obtained only 20 to 30 times out of 100 tests.

Table 17. D matrix for non-far field 2D case (meters).

	S1	S2	S3	S4	S5	S6
RX1	10.943	8.944	11.187	13.665	8.884	12.298
RX2	11.428	9.511	11.314	13.734	7.727	9.456
RX3	14.136	10.718	10.312	11.831	4.525	5.751
RX4	14.502	10.486	9.136	10.541	3.568	8.958
RX5	9.740	5.138	6.153	9.246	8.386	15.363
RX6	5.997	5.220	9.379	12.330	9.873	15.116

In figure 24, signs in red indicate the designated TX, RX and Scatter positions while blue signs indicate the reconstructed ones. The designated positions are the given in table 5, 6 and 7 in Chapter 3. The measured positions, by running P410 range request, are not considered in order to avoid the inter-error, because that the measurement are carried out by P410 units, and the D_d_signal in table 17 are obtained from P410 units as well. From figure 24, all the positions of TX, RXs and Scatterers are approximately matched: accurate match could be observed from RX4, RX5,

RX6, S2, S3, S4, and S5; while mismatch deviation for TX, RX1, RX3, S1 and S6 are around 5 to 15 cm, and error for RX2 is around 20 to 27 cm.

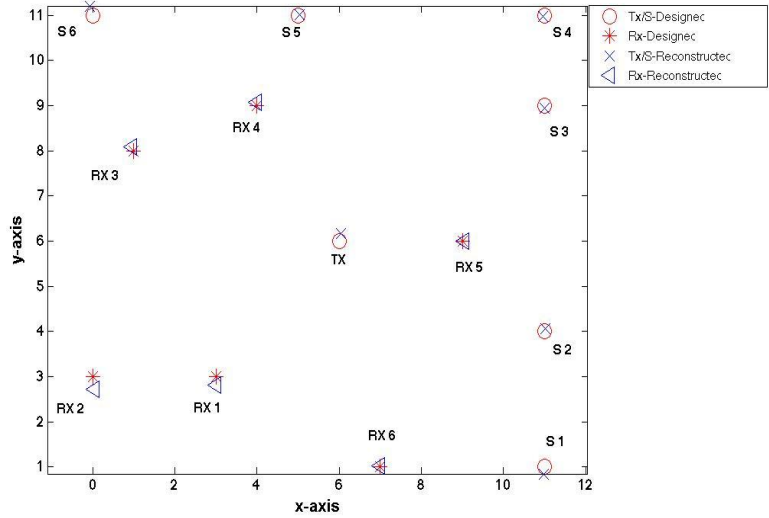


Figure 24. Position estimates comparison | non-far field 2D case.

The least error in the non-far field case is 0.0360 m, while the largest is 0.2788 m. Compared to the largest test dimension 12 m, the relative error is around 0.3% to 2.3%, which is a reasonable and convincing result.

The error may firstly come from inevitable errors by ruler measurements; secondly, it may be brought by D_d_signal calculations; last by not least, the position estimation algorithm will lead to errors.

4.2 Position estimates of the 2D case

The D matrix in table 18 is the D_d_signal of the estimation for 2D case in meter for all the RXs, they are used to reconstructed positions of TX, RXs and Scatterers. Reconstructed positions are processed by FFUTOA algorithm. 2D case position estimates could be completed using a pre-initialized s_j and r_i value to start with.

Table 18. D matrix for 2D case (meters).

	S1	S2	S3	S4	S5	S6
RX1	13,528	14,795	18,908	17,312	16,543	16,584
RX2	9,072	10,504	15,578	15,010	15,811	17,554
RX3	10,989	11,254	15,093	13,752	14,352	16,205
RX4	12,174	11,456	14,333	11,689	11,483	13,363
RX5	14,553	14,352	17,431	14,466	12,531	12,426

RX6	14,553	14,869	18,936	16,319	14,425	13,496
-----	--------	--------	--------	--------	--------	--------

In figure 25, shapes in red indicate the designated TX, RXs and the Scatters positions; the blue shape indicates the reconstructed ones. The designated positions are the designated positions in table 9, 10 and 11. There are measurements by the ruler and by the laser meter in tables, but only measurements by the laser meter are considered since it is considered to have better accuracy.

As shown in figure 25, all the positions of TX, RXs and Scatterers are roughly paired and with reasonable approximation. Quite accurate matches could be observed from RX2, RX3 and S5 whose deviations are around 4 to 11 cm; while the mismatch for TX, RX1, RX4, S1, S2, S3, S4 and S6 are around 17 to 28 cm, and error for RX5 and RX6 are around 33 to 44 cm.

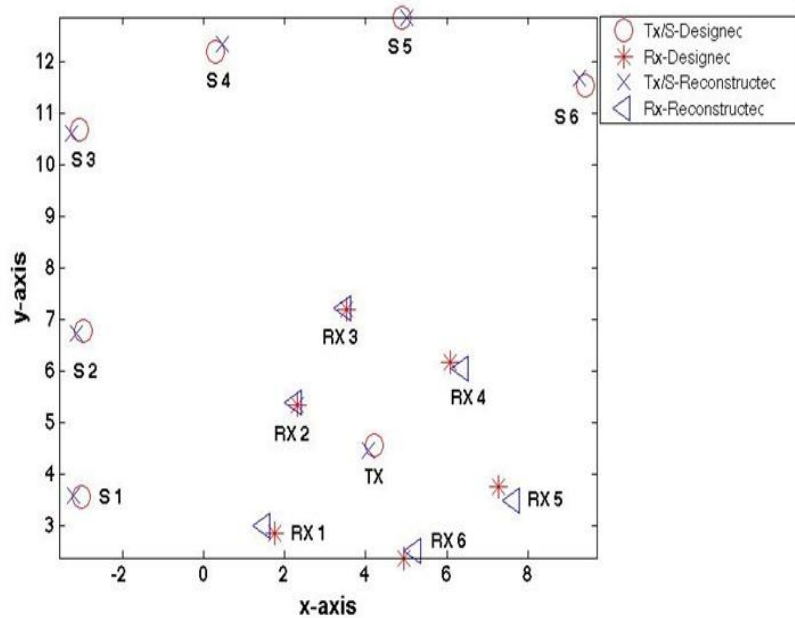


Figure 25. Position estimates comparison | 2D case.

The least value for the mismatch in the 2D case is 0.044 m, while the largest value is 0.441 m. Compared to the test dimension 12.9 m, the relative error is around 0.34% to 3.4%, which is a reasonable and expected result.

As in the non-far field 2D case, the error may firstly come from inevitable errors by measurements. Secondly, it may be caused by

D_d_signal calculations. Last but not least, the position estimation algorithm will lead to errors.

4.3 Position estimates of the 2D far field case

Table 19 shows the D matrix, which is the D_d_signal estimation for 2D far field case in meter, the D matrix are used to reconstructed positions of TX, RXs and Scatterers. Reconstructed positions are processed by algorithm described in Chapter 2. 2D far field case position estimates could be completed using a pre-initialized s_j and r_i value.

Table 19. D matrix for the algorithm of 2D far field case (meters).

	S1	S2	S3	S4	S5	S6	S7	S8	S9
RX1	14,992	13,777	18,329	21,228	19,994	None	16,977	16,117	17,468
RX2	15,552	13,061	17,126	19,782	19,260	None	18,035	17,647	18,784
RX3	17,336	14,450	17,742	18,918	17,467	None	17,446	17,967	19,974
RX4	18,013	15,771	19,340	20,151	17,129	None	15,808	16,705	19,420
RX5	17,430	15,916	19,997	21,315	18,15	None	15,029	15,445	18,126
RX6	16,104	15,106	19,623	21,887	19,538	None	15,695	15,155	17,143

Figure 26 shows comparisons of designated positions and reconstructed ones, as similar analysis above for non-far field and 2D cases. Shapes in red indicate the designated TX RXs and Scatterers positions while blue shape indicates the reconstructed ones. The designated positions are the designated positions in table 13, 14 and 15. Measurements by ruler are not used in comparison since laser meter measurements are more accurate.

As shown in figure 26, all the positions of TX, RXs and Scatterers are roughly matched and with reasonable values. S6 is not taken into account. As could be observed, RXs as designated are roughly around a circle, and scatterers are located in approximately all directions. Good matches could be observed from S1 and S5 whose deviations are around 9 to 16 cm; while the mismatch for TX, RX1, RX2, RX3, RX4, RX5 and RX6 are around 26 to 37 cm, and error for S2, S3, S4, S5, S7, S8 and S9 are around 49 to 86 cm.

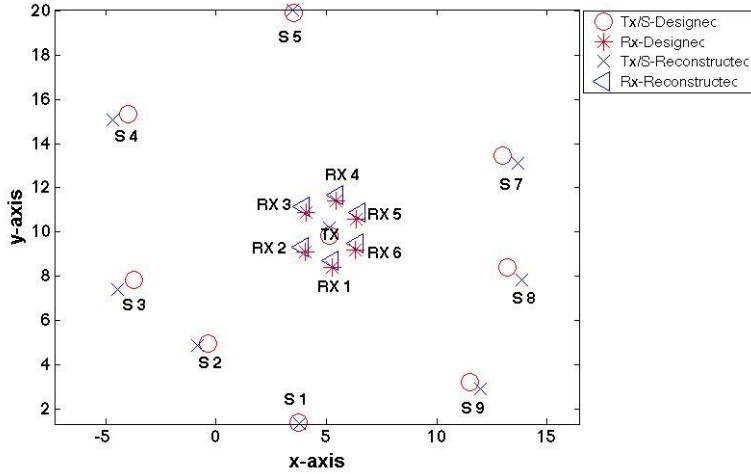


Figure 25. Position estimates comparison | 2D far field case.

The least value for the mismatch in the 2D far field case is 0.091 m, while the largest value is 0.866 m. Compared to the test dimension 20 m, the relative error is around 0.45% to 4.3%, which is a reasonable and expected result due to the large test setup dimension.

Similar to non-far field and 2D case, the error may firstly come from inevitable errors by measurements; secondly, it may be caused by D_d_signal calculations; last by not least, the position estimates algorithm will lead to errors.

CHAPTER 5

5 Discussions of 2D/3D far field case

In this chapter, the 2D/3D far field experiment is introduced, as well as the results and future improvements.

5.1 2D/3D far field case

The antenna pattern in figure 26 shows that P410 units are capable of transmitting as well as receiving signals in three dimensions. Thus, a 2D/3D far field measurement is carried out. 2D indicates TX and Scatterers are located in the ground plane, 3D indicates several RXs are located in three dimensions.

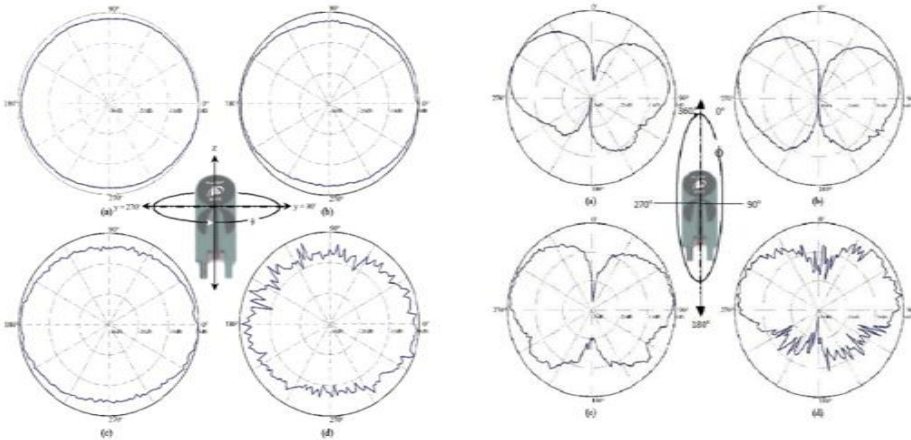


Figure 26. Antenna pattern of the P410 unit [34].

2D/3D far field test is the extended experiment of the 2D far field case described in Chapter 3. The only difference between 2D far field and 2D/3D far field is that in the 2D/3D far field case, RX1, RX2, RX4, and RX5 are fixed on a pole at roughly the same spot as in the 2D far field case, thus introducing a z-axis data displacement. The z-axis data for the four receivers are given in tables in Appendix 3. Figure 27 shows the measurement environment of TX and RXs positions for this case.



Figure 27. TX and RXs positions for 2D/3D case.

As mentioned above, RX1/RX2/RX4/RX5 are the units, which have a z-axis displacement, while RX3 and RX6 remain at the same positions as in the 2D far field case. Figure 28 shows the receive signal for RX1. Results for other receivers are listed in Appendix 3. As shown in figure 28, for RX1 there exists no obvious reflection from scatterers; results listed in Appendix 4 for RX2/RX4/RX5 are similar with RX1. For two RXs (RX3 and RX6), since they are put in the same ground plane as TX and scatterers, the receive signals indicate similar results as the 2D far field case. The scattered path is hard to observe from the received signals for the rest receivers; several stable scatterers, which maybe the other 3 poles used to hold units around time 10 to 20 ns in figure 28. The result may be due to the characteristics of the pipe—it has a high possibility to have weak reflections in directions apart from the horizontal plane.

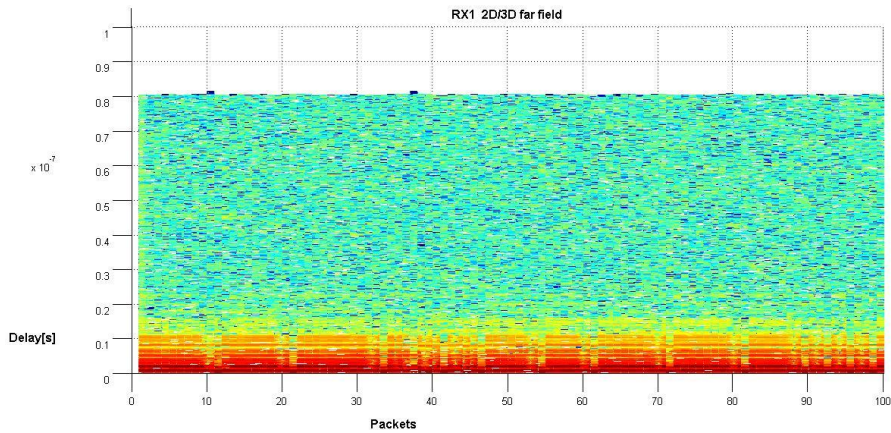


Figure 28. RX1 2D/3D far field case.

The steel bowl in figure 29 gives a higher reflection in the whole upper unit sphere than the pipe. After changing the pipe to a big steel bowl, another test is carried out. There are one TX, 1 RX and nine scatterer positions. The distance between TX and RX is 1.5 m. The RX is placed on the pole, with a height of 3.658 m. The nine scatterers are located in all directions. The distance of TX and RX to all scatterers are recorded in table 20, the data is measured using the laser meter.



Figure 29. Steel bowl as scatterer.

Table 20. TX and RX to all scatterers for 2D/3D far field 1TX 2RX test (meters).

	S1	S2	S3	S4	S5	S6	S7	S8	S9
TX	6.025	9.187	8.927	8.088	9.633	9.148	7.822	6.250	7.348
RX	5.817	7.939	7.213	6.450	8.003	8.823	8.809	7.752	8.534

As figure 30 shows, there are at least six scatterers, however, the amplitude of only two of them is obvious, and others are quite weak. Table 20 indicates the distance for the transmit signal sending from TX to scatterers and then reflecting back to RX. For example, the D for S1 is 10.342 m.

In conclusion, one TX and 1 RX 2D/3D far field case proves that a better reflector do improve the receive signal SNR, however, the steel bowl as the reflector is still not good enough for the far field test. As mentioned in chapter 2, the far field test may require the distance of RX to scatterer be at least 4 times longer than the distance of TX to RX. However, with the distance like this, the signal reflected decay too much before it arrives to RX.

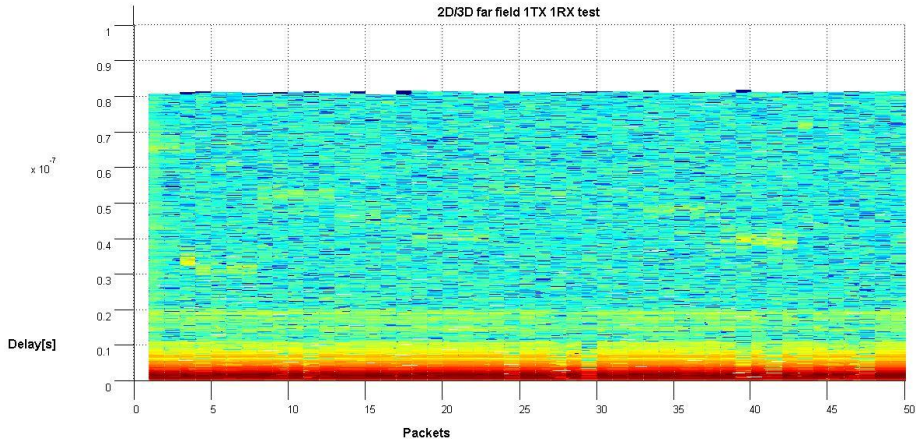


Figure 30. 2D/3D far field test with 1TX, 1RX, 9 Scatterer positions.

CHAPTER 6

6 Conclusions and improvements

In this thesis, the sensor localization using UWB signals in unsynchronized scenario has been studied. Three outdoor measurements have been performed.

Estimates from the non-far field 2D case show the possibility to localize nodes in random distribution. The 2D case and 2D far field case show that the FFUTOA algorithm is stable and give reliable results. Results presented in Chapter 4 shows that the reconstructed positions approximately match. Among all the three cases, the least error in cm is 3.6 cm of non-far field 2D case, and the largest deviation is 86 cm in 2D far field case. Although the 2D far field case has the largest deviation, it has a maximum relative error of around 4.3%, which is good considering large dimensions situation.

The comparison between 2D case and 2D far field case shows that the position of the nodes still can be obtained even though the setup does not fulfill the far field assumption.

The time-based positioning scheme based on UWB signals performs better compared to most of the conventional positioning schemes

Its main drawbacks are: precise calibrations and measures of the dimensions for each case are needed, which add complexity on the practical situation; the other is that none of the three implementations are full automatic.

The next step would be continue the 2D/3D far field test but with a better reflector. With a better receive signal SNR, implementation of the 2D/3D far field algorithm would be possible. An interesting case worth study would be the 3D case.

Furthermore, it would be interesting to make a self-organized network formed by units, which means all the sensors collect, analyze and process the position automatically.

References

1. Vossiek, M., et al., *Wireless local positioning*. Microwave Magazine, IEEE, 2003. **4**(4): p. 77-86.
2. Drane, C., M. Macnaughtan, and C. Scott, *Positioning GSM telephones*. Communications Magazine, IEEE, 1998. **36**(4): p. 46-54, 59.
3. Caffery, J.J. and G.L. Stuber, *Overview of radiolocation in CDMA cellular systems*. Communications Magazine, IEEE, 1998. **36**(4): p. 38-45.
4. Ludden, B. and L. Lopes. *Cellular based location technologies for UMTS: a comparison between IPDL and TA-IPDL*. in *Vehicular Technology Conference Proceedings, 2000. VTC 2000-Spring Tokyo. 2000 IEEE 51st*. 2000.
5. Enge, P., *The Global Positioning System: Signals, measurements, and performance*. International Journal of Wireless Information Networks, 1994. **1**(2): p. 83-105.
6. Ross, G.F., *The Transient Analysis of Certain TEM Mode Four-Port Networks*. Microwave Theory and Techniques, IEEE Transactions on, 1966. **14**(11): p. 528-542.
7. Gezici, S. and H.V. Poor, *Position Estimation via Ultra-Wide-Band Signals*. Proceedings of the IEEE, 2009. **97**(2): p. 386-403.
8. Federal, Communications, and Commission, *First report and order 02-48*. 2002.
9. Guvenc, I., S. Gezici, and Z. Sahinoglu. *Ultra-wideband range estimation: Theoretical limits and practical algorithms*. in *Ultra-Wideband, 2008. ICUWB 2008. IEEE International Conference on*. 2008. IEEE.
10. Win, M.Z. and R.A. Scholtz, *Impulse radio: how it works*. Communications Letters, IEEE, 1998. **2**(2): p. 36-38.
11. Gezici, S., et al., *Localization via ultra-wideband radios: a look at positioning aspects for future sensor networks*. Signal Processing Magazine, IEEE, 2005. **22**(4): p. 70-84.
12. Siwiak, K. and J. Gabig. *IEEE 802.15.4IGa informal call for application response, contribution #11*. [cited 2013 Sep]; Available from: <http://www.ieee802.org/15/pub/TG4a.html>.

-
13. Timedomain, *Time Domain's Ultra Wideband (UWB) Definition & Advantages*, 2012.
 14. Gezici, S., *A Survey on Wireless Position Estimation*. Wireless Personal Communications, 2008. **44**(3): p. 263-282.
 15. Gustafsson, F. and F. Gunnarsson, *Mobile positioning using wireless networks: possibilities and fundamental limitations based on available wireless network measurements*. Signal Processing Magazine, IEEE, 2005. **22**(4): p. 41-53.
 16. Weiss, A.J., *Direct position determination of narrowband radio frequency transmitters*. Signal Processing Letters, IEEE, 2004. **11**(5): p. 513-516.
 17. Caffery, J.J., *Wireless Location in CDMA Cellular Radio Systems*. 2000, Boston: MA: Kluwer Academic.
 18. Patwari, N., et al., *Locating the nodes: cooperative localization in wireless sensor networks*. Signal Processing Magazine, IEEE, 2005. **22**(4): p. 54-69.
 19. Yihong, Q. and H. Kobayashi. *On relation among time delay and signal strength based geolocation methods*. in *Global Telecommunications Conference, 2003. GLOBECOM '03. IEEE*. 2003.
 20. Joon-Yong, L. and R.A. Scholtz, *Ranging in a dense multipath environment using an UWB radio link*. Selected Areas in Communications, IEEE Journal on, 2002. **20**(9): p. 1677-1683.
 21. Lindsey, W.C. and M.K. Simon, *Phase and Doppler Measurements in Two-Way Phase-Coherent Tracking Systems*. New York: Dover, 1991.
 22. Turin, G., *An introduction to matched filters*. Information Theory, IRE Transactions on, 1960. **6**(3): p. 311-329.
 23. Pallas, M.A. and G. Jourdain, *Active high resolution time delay estimation for large BT signals*. Signal Processing, IEEE Transactions on, 1991. **39**(4): p. 781-788.
 24. Poor, H.V., *An Introduction to Signal Detection and Estimation*. 1994, New York: Springer-Verlag.
 25. Cook, C.E. and M. Bernfeld, *Radar Signals: An Introduction to Theory and Applications*. 1970, New York: Academic.
 26. Caffery, J. and G.L. Stuber, *Subscriber location in CDMA cellular networks*. Vehicular Technology, IEEE Transactions on, 1998. **47**(2): p. 406-416.

-
27. Yilin, Z., *Standardization of mobile phone positioning for 3G systems*. Communications Magazine, IEEE, 2002. **40**(7): p. 108-116.
 28. Yan, J., *Algorithms for indoor positioning systems using ultra-wideband signals*. 2010: Delft University of Technology.
 29. Mallat, A., J. Louveaux, and L. Vandendorpe. *UWB Based Positioning in Multipath Channels: CRBs for AOA and for Hybrid TOA-AOA Based Methods*. in *Communications, 2007. ICC '07. IEEE International Conference on*. 2007.
 30. Y. Kuang, K. Åström, and F. Tufvesson, *Single antenna anchor-free UWB positioning based on multipath propagation*, in *Proc. IEE International Conference on Communications 2013*: Budapest, Hungary.
 31. S. Burgess, Y. Kuang, and J. Wendeborg, *Minimal Solvers for Unsynchronized TDOA Sensor Network Calibration using Far Field Approximation*. 2013.
 32. Timedomain, *CAT User Guide*, 2012.
 33. Timedomain, *RCM RET User Guide*, 2012.
 34. Timedomain, *Broadspec Antenna Product Brochure*, 2011.

Appendix

A.1 Measured data and received signals for non-far field 2D case

This part describes distances of the test environment measured by a ruler as well as range request [33] of P410 units, and the received signals of RX1 to RX6 for the non-far field 2D case.

A.1.1 Measured data

The following tables show TX, each RX and Scatterer positions and distances in between. Ruler is used for building the coordinate system in the open field. Distances between TX, RX and Scatterers are not measured by the ruler. Instead, they are calculated from the positions of TX, RXs and Scatterers in the coordinate system. Those distances are recorded as designated distance in the following tables. Due to reasons like 1) the open field is not absolutely flat; 2) ruler data are not accurate enough due to rounding; 3) rounding in the calculation, there appears to be some inevitable error. There is one more item called measured distance in the table, which means the data recorded by range request. As mentioned in [33], the accuracy of the range request is millimeter. It would bring some inevitable error.

Table 1. The distance (meter) from TX to all RXs (meters).

	RX1	RX2	RX3	RX4	RX5	RX6
Designated	4.242	6.708	5.385	3.605	3	5.099
Measured	4.45	6.942	5.278	3.397	2.950	5.282

Table 2 shows the distance from TX to all S1 to S6.

Table 2. Distance (meter) from TX to all Scatterers (S1-S6) (meters).

	S1	S2	S3	S4	S5	S6
Designated	7.701	5.385	5.830	7.071	5.099	7.8102
Measured	7.162	5.406	5.634	6.737	4.839	7.702

Table 3 shows the distance from each RX to each Scatterer.

Table 3. Distance (meter) from all RX to all Scatterers (meters).

	S1	S2	S3	S4	S5	S6
RX1_Designated	8.246	8.062	10	11.313	8.246	8.544
RX1_Measured	8.159	8.067	9.951	11.274	8.316	8.707
RX2_Designated	11.18	11.045	12.530	13.601	9.434	8
RX2_Measured	11.22	11.024	12.617	13.673	9.561	8.195
RX3_Designated	12.20	10.770	10.050	10.443	5	3.162
RX3_Measured	12.21	10.676	9.979	10.270	5.139	3.105
RX4_Designated	10.63	8.602	6.964	7.280	2.236	4.472
RX4_Measured	10.92	8.519	6.964	7.102	2.217	4.521
RX5_Designated	5.385	2.828	3.606	5.3852	6.403	10.295
RX5_Measured	5.377	2.762	3.410	5.187	6.398	10.320
RX6_Designated	4	5	8.943	10.770	10.198	12.206
RX6_Measured	4.017	5.023	8.910	10.724	10.207	12.06

A.1.2 Received signals

The following twelve figures are the receive signals of RX1 to RX6. LOS components in all RXs are aligned by Matlab.

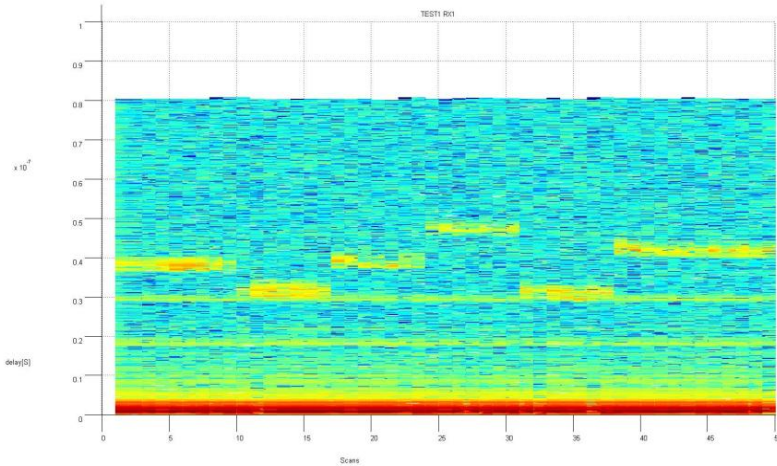


Figure 1. Received signals of RX1 | non-far field 2D case.

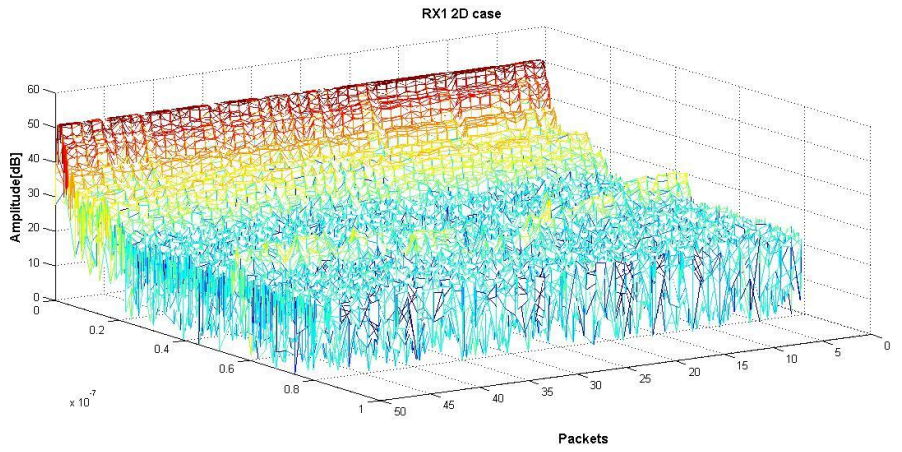


Figure 2. Received signals (2) of RX1 | non-far field 2D case.

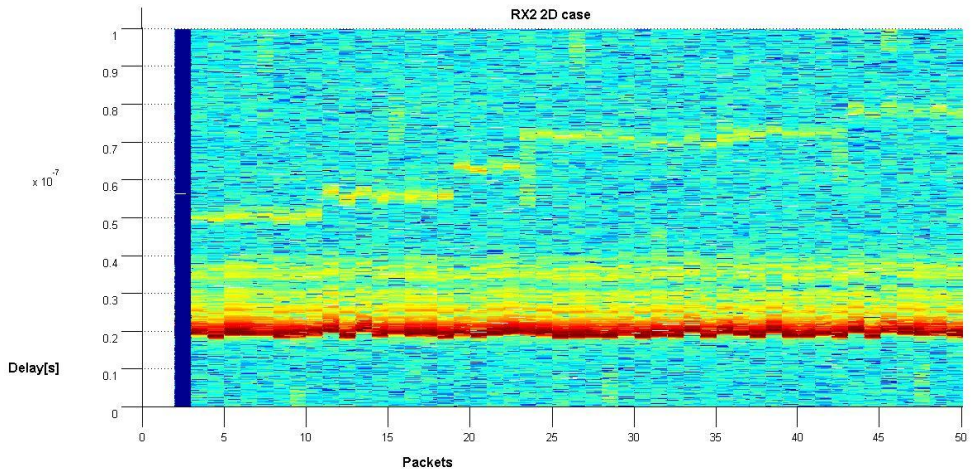


Figure 3. Received signals of RX2 | 2D case.

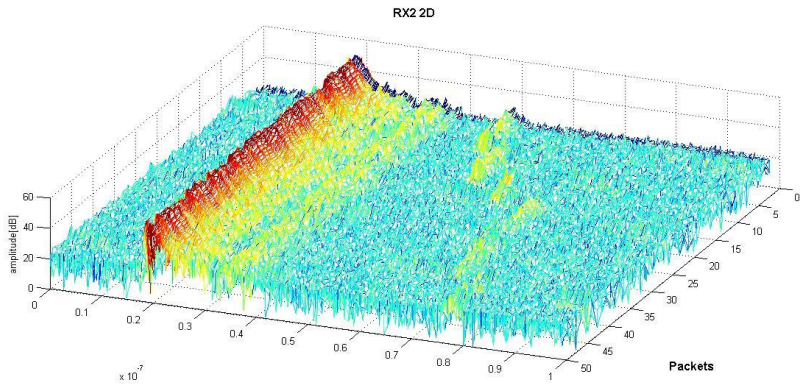


Figure 4. Received signals (2) of RX2 | 2D case.

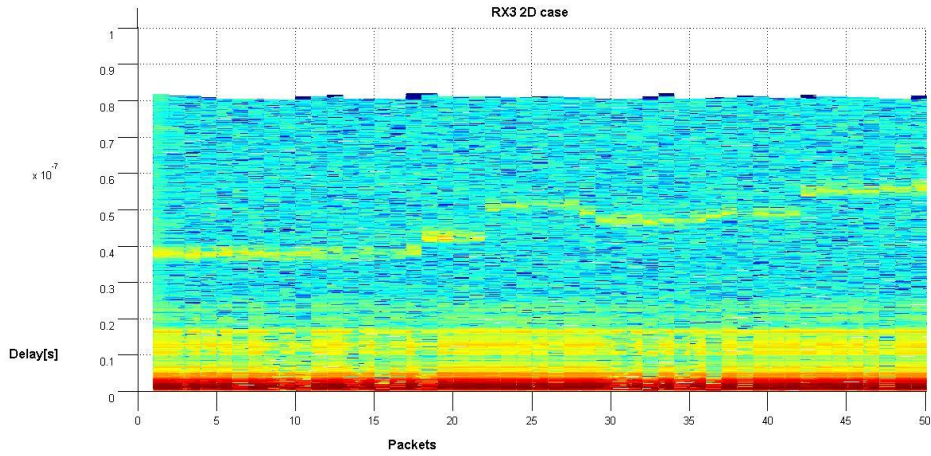


Figure 5. Received signals of RX3 | 2D case.

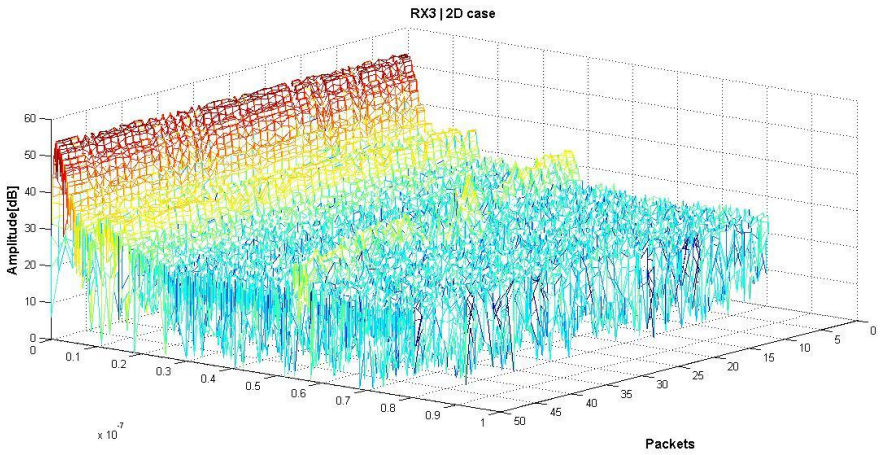


Figure 6. Received signals (2) of RX3 | 2D case.

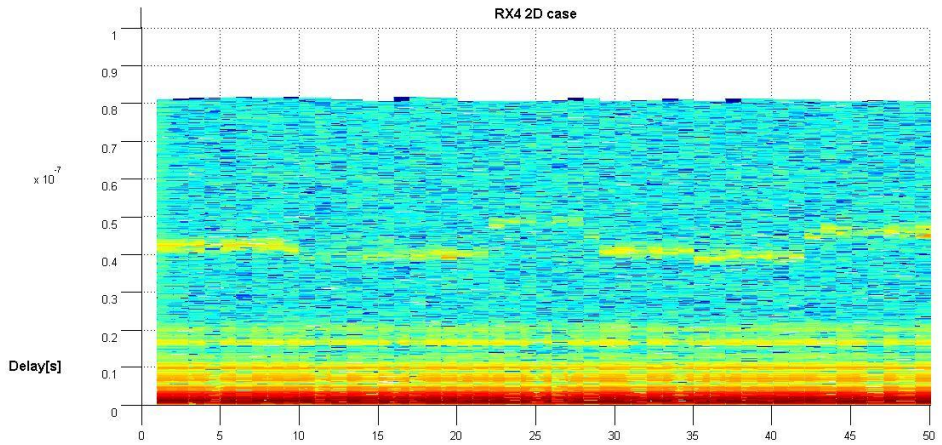


Figure 7. Received signals of RX4 | 2D case.

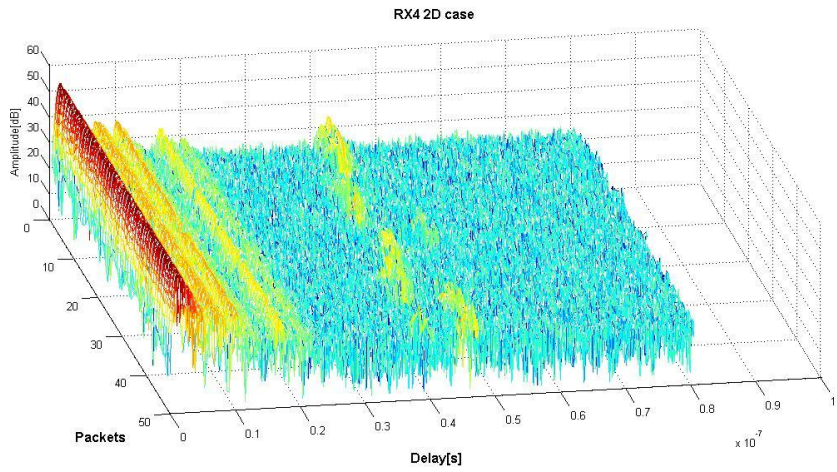


Figure 8. Received signals (2) of RX4 | 2D case.

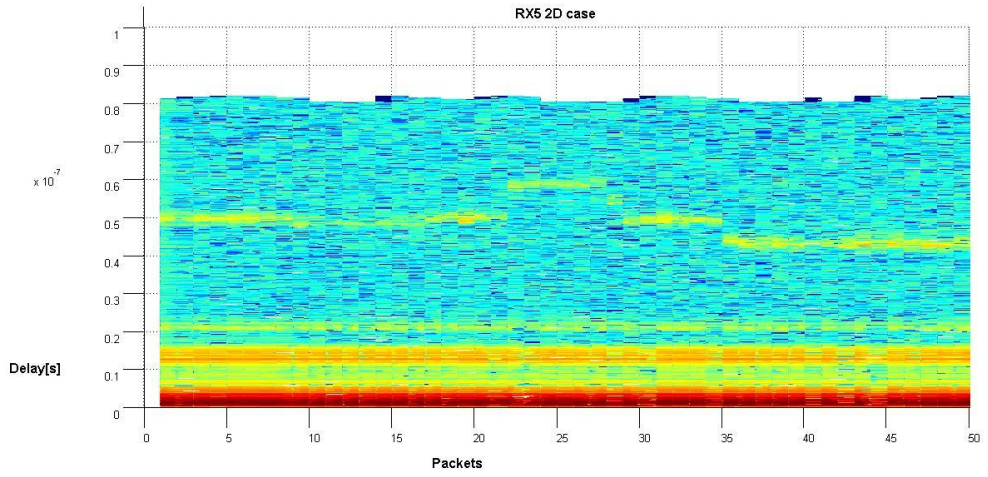


Figure 9. Received signals of RX5 | 2D case.

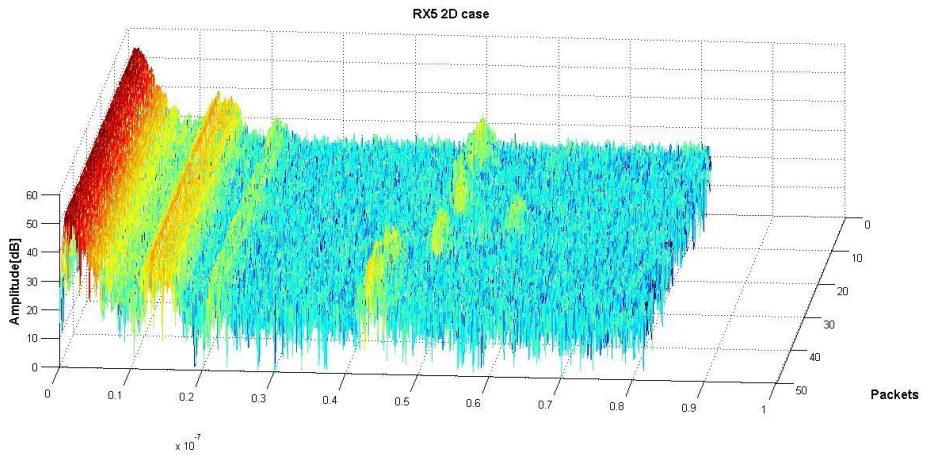


Figure 10. Received signals (2) of RX5 | 2D case.

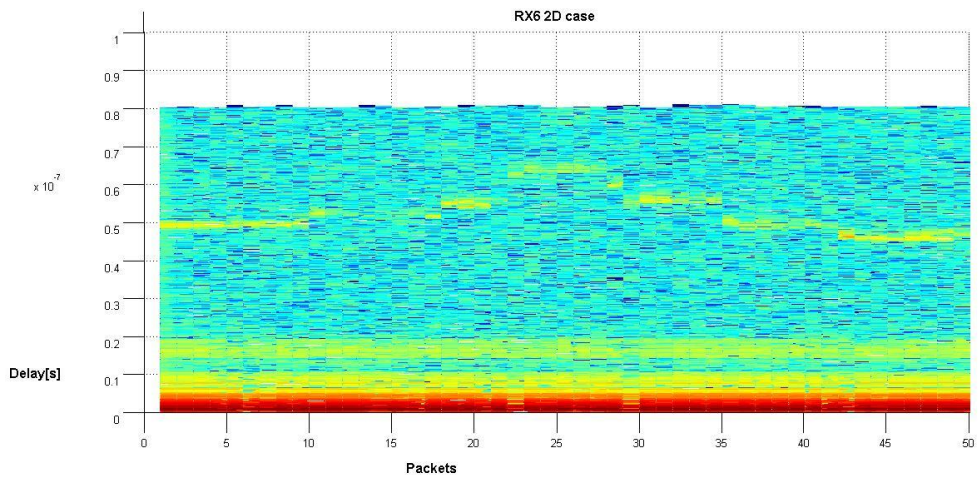


Figure 11. Received signals of RX6 | 2D case.

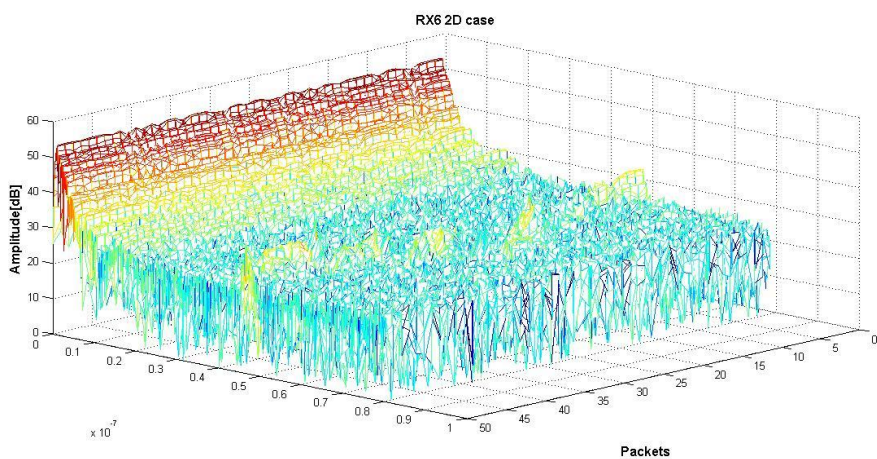


Figure 12. Received signals (2) of RX6 | 2D case.

A.1.3 Different distance

Table 6. Dd (meter) for RX1 | non-far field 2D case (meters).

For RX1	Dd_designated	Dd_measured	Dd_signal
S1	11.074	10.871	10.943
S2	9.204	9.023	8.944
S3	11.588	11.135	11.187

S4	11.142	13.561	13.665
S5	9.102	8.705	8.884
S6	12.116	11.959	12.298

Table 7. Dd (meter) for RX2 | non-far field 2D case (meters).

For RX2	Dd_designated	Dd_measured	Dd_signal
S1	11.543	11.442	11.428
S2	9.722	9.468	9.511
S3	11.652	11.309	11.314
S4	13.964	13.468	13.743
S5	7.824	7.478	7.727
S6	9.102	8.955	9.456

Table 8. Dd (meter) for RX3 | non-far field 2D case (meters).

For RX3	Dd_designated	Dd_measured	Dd_signal
S1	13.892	14.09	14.136
S2	10.770	10.804	10.718
S3	10.496	10.335	10.312
S4	12.126	11.729	11.831
S5	4.718	4.7	4.525
S6	5.587	5.529	5.751

Table 9. Dd (meter) for RX4 | non-far field 2D case (meters).

For RX4	Dd_designated	Dd_measured	Dd_signal
S1	14.096	14.68	14.502
S2	10.382	10.528	10.486
S3	9.225	9.201	9.136
S4	10.745	10.442	10.541
S5	3.725	3.659	3.568
S6	8.677	8.826	8.958

Table 10. Dd (meter) for RX5 | non-far field 2D case (meters).

For RX5	Dd_designated	Dd_measured	Dd_signal
S1	9.456	9.589	9.740
S2	5.213	5.218	5.138
S3	6.436	6.094	6.153

S4	9.456	8.974	9.246
S5	8.502	8.278	8.386
S6	15.105	15.072	15.363

Table 11. Dd (meter) for RX6 | non-far field 2D case (meters).

For RX6	Dd_designated	Dd_measured	Dd_signal
S1	5.973	5.951	5.998
S2	5.286	5.147	5.220
S3	9.676	9.262	9.379
S4	12.742	12.179	12.330
S5	10.198	9.764	9.873
S6	14.978	14.626	15.116

Appendix 2

A.2 Measured data and received signals for 2D case

This part includes dimensions of the test environment measured by ruler as well as the laser meter, and the received signals of RX1 to RX6 for 2D case.

A.2.1 Measured data

The following tables show distances between TX/RXs/Scatterers and Ref1/Ref2, TX and RXs, TX and Scatterers, RXs and Scatterers. The ruler and laser meter are used to do measurements. When use laser meter to measure distance, since the default reference point is at the back of the laser meter, but it is used to point the front edge of the laser meter to the place where the measurement should begin, that brings around 0.1480 m more in the recorded data of laser meter. Distance between Ref1 to Ref2 measured by the ruler is 11m, by the laser meter it is 11.115 m.

Table 1. The distance from TX to Ref1/Ref2, measured by ruler as well as the laser meter (meters).

	TX-Ref1	TX-Ref2
Ruler	6.23	8.19
Laser meter	6.360	8.294

Table 2. The distance from RXs to Ref1/ Ref2, measured by ruler as well as the laser meter(meters).

	RX1	RX2	RX3	RX4	RX5	RX6
Ref1_Ruler	5.52	3.41	5.88	8.08	8.71	8.25
Ref1_Laser meter	5.641	3.527	5.956	8.170	8.805	8.337
Ref2_Ruler	6.50	9.68	10.21	10.40	7.92	5.30
Ref2_Laser meter	6.623	9.805	10.324	10.503	8.024	5.419

Table 3. The distance from Scatterers (S1-S6) to Ref1/Ref2, measured by ruler and laser meter(meters).

	S1	S2	S3	S4	S5	S6
Ref1_Ruler	4.72	7.40	11.13	12.26	13.80	14.90
Ref1_Laser meter	4.836	7.551	11.266	12.343	13.903	15.031
Ref2_Ruler	14.46	15.55	17.69	16.24	14.27	11.66
Ref2_Laser meter	14.594	15.656	17.785	16.353	14.364	11.777

Table 4. The distance from TX to Scatterers (S1-S6), measured by ruler and laser meter(meters).

	S1	S2	S3	S4	S5	S6
TX_ruler	7.39	7.60	9.53	8.58	8.31	8.70
TX_laser meter	7.515	7.722	9.651	8.684	8.460	8.848

Table 5. The distance from TX to RXs measured by ruler and laser meter (meters).

	RX1	RX2	RX3	RX4	RX5	RX6
TX_ruler	2.14	3.32	2.11	2.78	2.55	3.25
TX_laser meter	2.269	3.415	2.211	2.931	2.683	3.354

Table 6. The distance from RXs to Scatterers (S1-S6), measured by ruler and laser meter (meters).

	S1	S2	S3	S4	S5	S6
RX1_ruler	8.08	9.02	11.40	10.68	10.29	10.01
RX1_laser meter	8.179	9.132	11.530	10.827	10.383	10.133
RX2_ruler	4.81	6.05	9.05	9.32	10.38	11.54
RX2_laser meter	4.944	6.172	9.198	9.476	10.511	11.658
RX3_ruler	5.67	5.49	7.51	7.09	7.95	9.48
RX3_laser meter	5.782	5.617	7.651	7.254	8.083	9.615
RX4_ruler	7.61	6.64	7.48	5.90	5.78	7.31
RX4_laser meter	7.753	6.766	7.609	6.042	5.897	7.478
RX5_ruler	9.60	9.25	10.29	8.34	6.74	6.22
RX5_laser meter	9.737	9.371	10.386	8.485	6.882	6.386
RX6_ruler	10.43	10.80	12.48	10.90	9.32	7.93
RX6_laser meter	10.562	10.938	12.597	11.402	9.429	8.069

A.2.2 Received signals

The following twelve figures are the receive signals of RX1 to RX6. LOS component in RX1, RX3, RX4, RX5 and RX6 are aligned by programming, while in RX2 are not aligned. This is because the not-aligned received signal shows better and more obvious results than the aligned one.

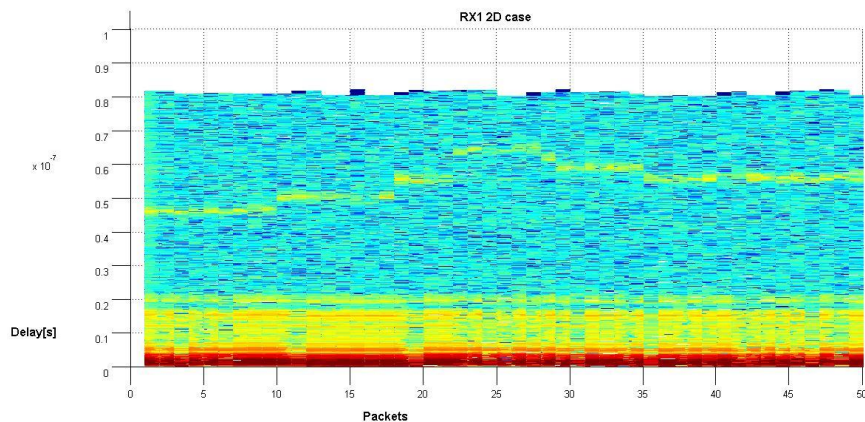


Figure 1. Received signals of RX1 | 2D case.

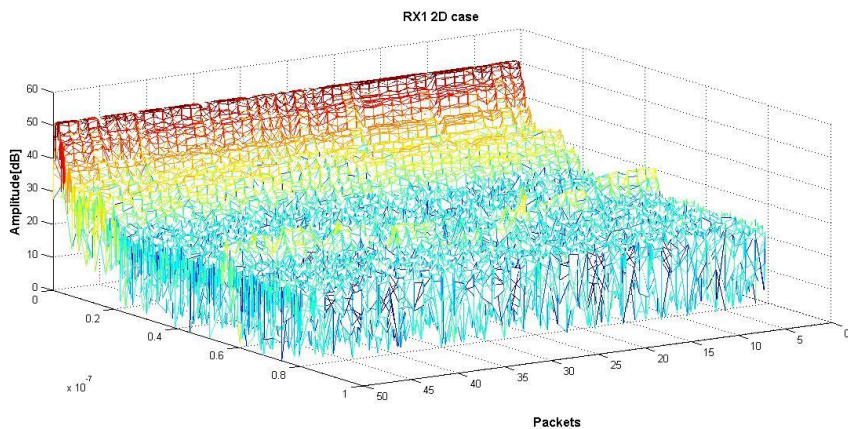


Figure 2. Received signals (2) of RX1 | 2D case.

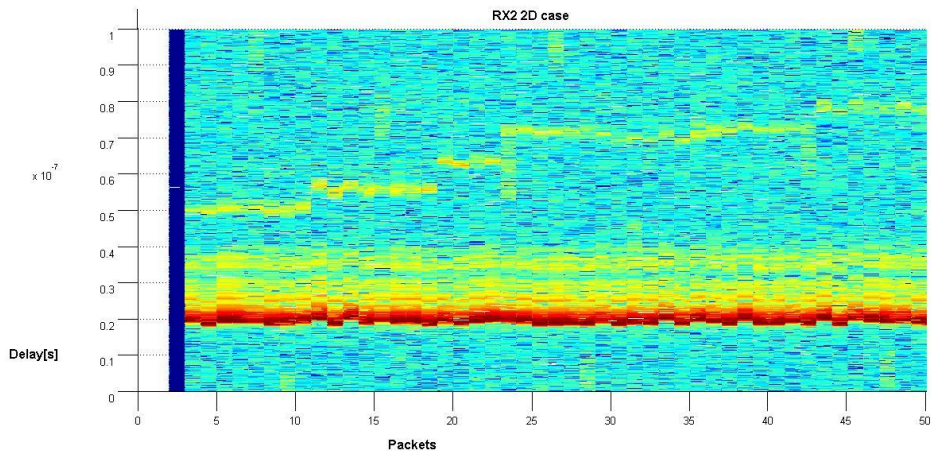


Figure 3. Received signals of RX2 | 2D case.

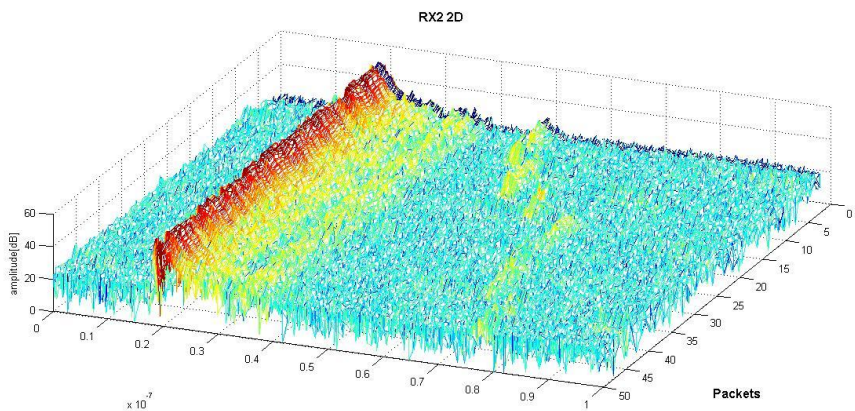


Figure 4. Received signals (2) of RX2 | 2D case.

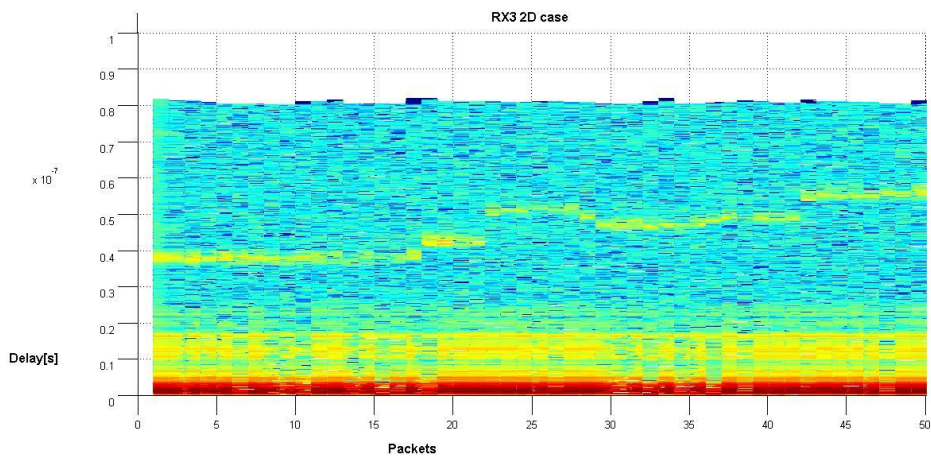


Figure 5. Received signals of RX3 | 2D case.

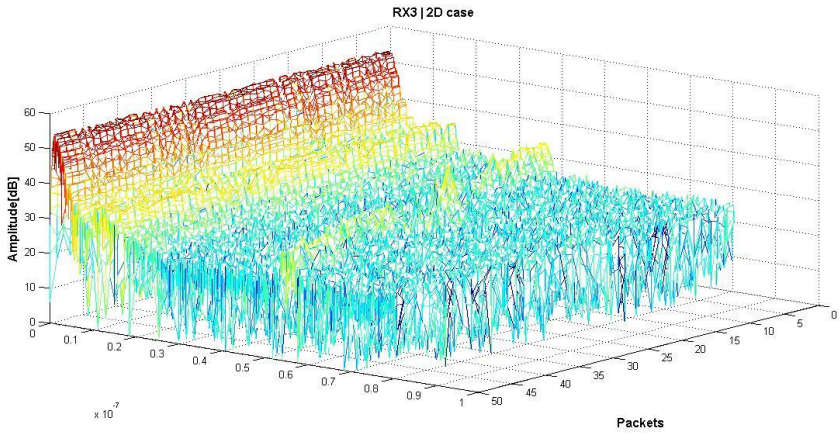


Figure 6. Received signals (2) of RX3 | 2D case.

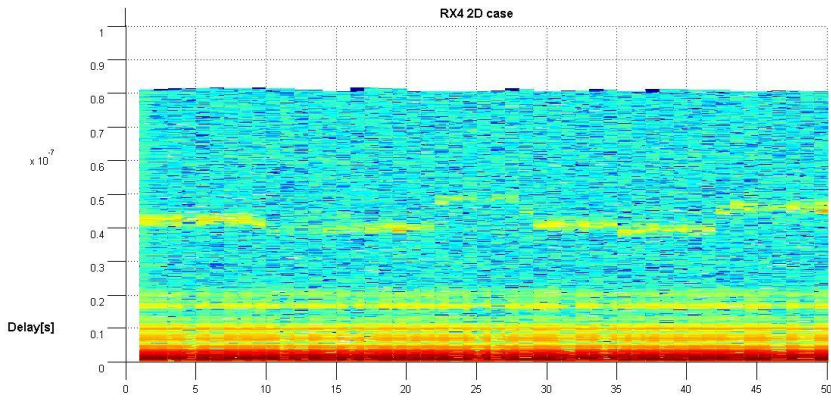


Figure 7. Received signals of RX4 | 2D case.

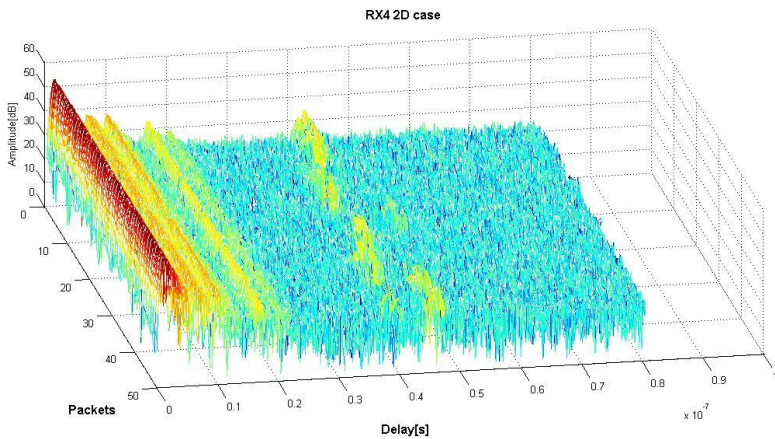


Figure 8. Received signals (2) of RX4 | 2D case.

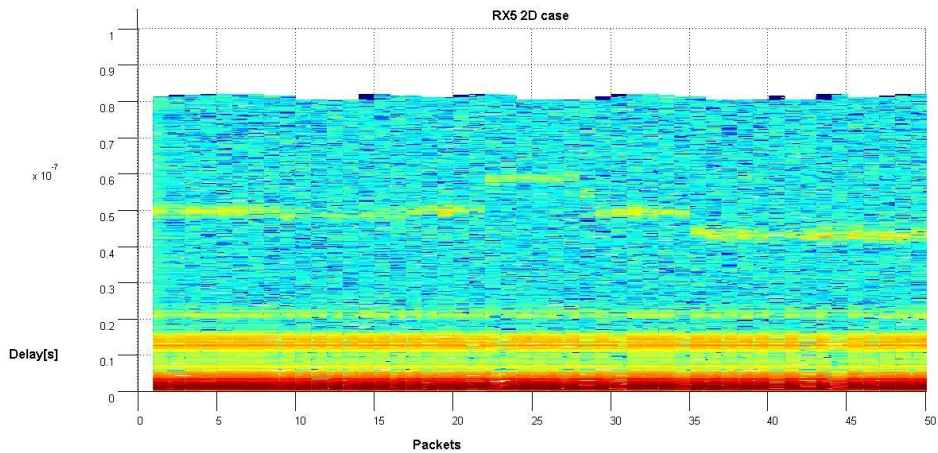


Figure 9. Received signals of RX5 | 2D case.

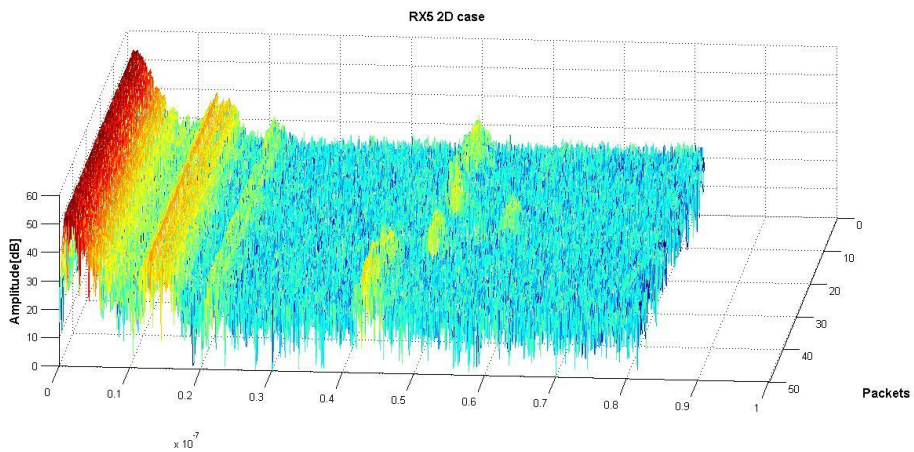


Figure 10. Received signals (2) of RX5 | 2D case.

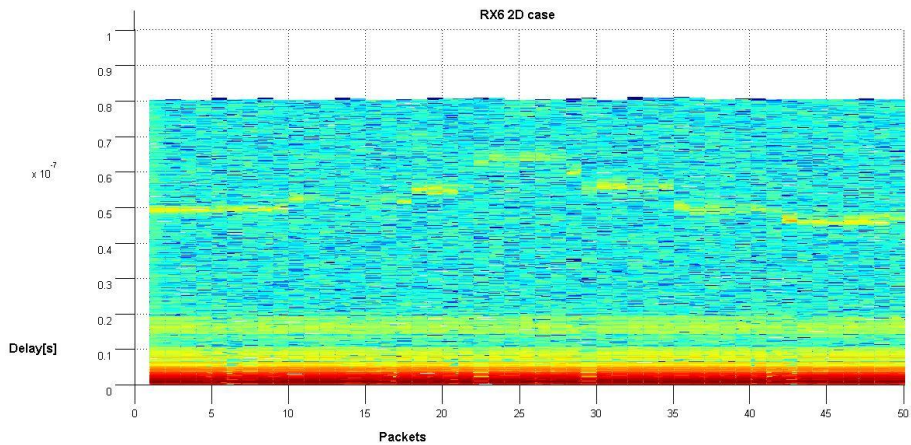


Figure 11. Received signals of RX6 | 2D case.

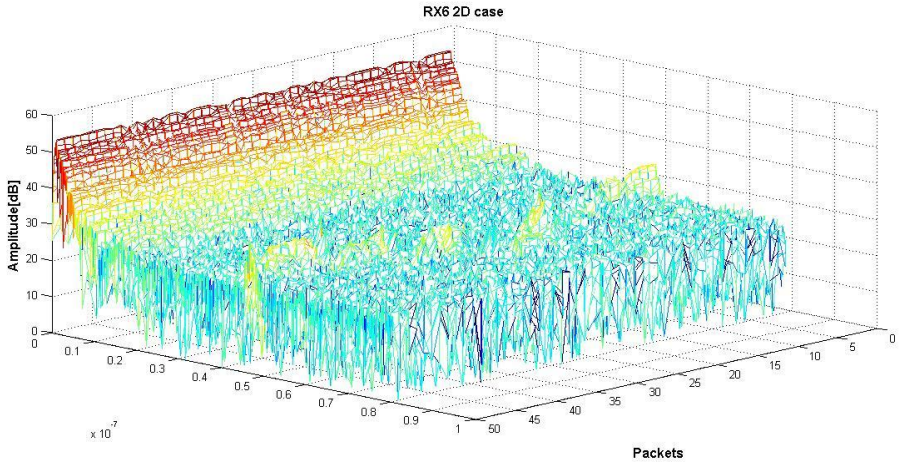


Figure 12. Received signals (2) of RX6 | 2D case.

A.2.3 Different distance

Table 7.the difference distance for RX1 (meters).

For RX1	Dd_ruler	Dd_laser	Dd_signal
S1	13,33	13,277	13.528
S2	14,48	14,437	14.795
S3	18,79	18,764	18.908
S4	17,12	17,094	17.312
S5	16,46	16,426	16.543
S6	16,57	16,564	16.584

Table 8. The difference distance for RX2 (meters).

For RX2	Dd_ruler	Dd_laser	Dd_signal
S1	8,88	8,896	9.0722
S2	10,33	10,331	10.504
S3	15,26	15,286	15.578
S4	14,58	14,597	15.011
S5	15,37	15,408	15.811
S6	16,92	16,943	17.554

Table 9. The difference distance for RX3 (meters).

For RX3	Dd_ruler	Dd_laser	Dd_signal
S1	10,95	10,938	10.989
S2	10,98	10,98	11.254
S3	14,93	14,943	15.093
S4	13,56	13,579	13.752
S5	14,15	14,184	14.352
S6	16,07	16,104	16.205

Table 10. The difference distance for RX4 | 2D case (meters).

For RX4	Dd_ruler	Dd_laser	Dd_signal
S1	12,22	12,189	12.174
S2	11,46	11,409	11.455
S3	14,23	14,181	14.333
S4	11,7	11,647	11.689
S5	11,31	11,278	11.483
S6	13,23	13,247	13.363

Table 11. The difference distance for RX5 (meters).

For RX5	Dd_ruler	Dd_laser	Dd_signal
S1	14,44	14,421	14.553
S2	14,3	14,262	14.352
S3	17,27	17,206	17.431
S4	14,37	14,338	14.466
S5	12,5	12,511	12.531
S6	12,37	12,403	12.425

Table 12. The difference distance for RX6 (meters).

For RX6	Dd_ruler	Dd_laser	Dd_signal
S1	14,57	14,575	14.553
S2	15,15	15,158	14.868
S3	18,76	18,746	18.936
S4	16,23	16,584	16.319
S5	14,38	14,387	14.425
S6	13,38	13,415	13.496

Appendix 3

A.3 Measured data and received signals for 2D far field case

This part includes distances in the test environment measured by a ruler as well as the laser meter, and the received signals of RX1 to RX6 for 2D far field case.

A.3.1 Measured data

The following tables show distances between TX/RXs/Scatterers and Ref1/Ref2, TX and RXs, TX and Scatterers, RXs and Scatterers. Data are the by a ruler and the laser meter. When using laser meter to measure distance, since the default reference point is at the back of the laser meter, but it is used to point the front edge of the laser meter to the place where the measurement should begin, that brings around 0.1480 m more in the recorded data of laser meter.

Table 1. The distance from TX to Ref1/Ref2, measured by ruler as well as the laser meter (meters).

	TX-Ref1	TX-Ref2
Ruler	11.19	11.46
Laser meter	11.352	11.618

Table 2. The distance from RXs to Ref1/ Ref2, measured by ruler as well as the laser meter (meters).

	RX1	RX2	RX3	RX4	RX5	RX6
Ref1_Ruler	9.92	9.94	11.64	12.645	12.38	11.16
Ref1_Laser meter	10.069	10.090	11.782	12.791	12.500	11.301
Ref2_Ruler	10.08	11.36	12.82	12.64	11.54	10.26
Ref2_Laser meter	10.218	11.501	12.959	12.783	11.655	10.393

Table 3. The distance from Scatterers (S1-S6) to Ref1/Ref2, measured by ruler and laser meter (meters).

	S1	S2	S3	S4	S5	S6	S7	S8	S9
Ref1_Ruler	3.46	4.95	8.65	15.83	20.23	23.19	18.69	15.67	11.91
Ref1_Laser meter	3.595	5.123	8.830	15.989	20.375	23.249	18.827	15.808	12.079
Ref2_Ruler	6.95	12.24	16.54	21.37	21.19	20.32	13.61	8.75	3.24
Ref2_Laser meter	7.110	12.382	16.682	21.471	21.362	20.504	13.770	8.912	3.437

Table 4. The distance from TX to Scatterers (S1-S6), measured by ruler and laser meter (meters).

	S1	S2	S3	S4	S5	S6	S7	S8	S9
TX_ruler	9	8	10	11	10	12	9	9	10
TX_laser meter	9.126	8.186	10.163	11.088	10.102	12.058	9.125	9.126	10.139

Table 5. The distance from TX to RXs measured by ruler and laser meter (meters).

	RX1	RX2	RX3	RX4	RX5	RX6
TX_ruler	1.5	1.5	1.5	1.5	1.5	1.5
TX_laser meter	1.640	1.640	1.605	1.639	1.641	1.637

Table 6. The distance from RXs to Scatterers (S1-S6), measured by ruler and laser meter (meters).

	S1	S2	S3	S4	S5	S6	S7	S8	S9
RX1_ruler	7.55	7.23	9.82	11.83	11.49	13.18	9.49	8.63	8.87
RX1_laser meter	7.732	7.388	10.018	11.997	11.613	13.300	9.653	8.772	9.016
RX2_ruler	8.10	6.55	8.60	10.38	10.73	13.31	10.43	10.02	10.31
RX2_laser meter	8.191	6.704	8.765	10.498	10.850	13.457	10.581	10.193	10.496
RX3_ruler	9.80	7.91	9.27	9.56	8.95	11.86	9.83	10.34	11.47
RX3_laser meter	9.941	8.053	9.447	9.712	9.121	12.001	9.986	10.49	11.612
RX4_ruler	10.46	9.24	10.82	10.74	8.62	10.58	8.32	9.16	10.91
RX4_laser meter	10.621	9.389	10.998	10.863	8.800	10.710	8.408	9.285	11.072
RX5_ruler	9.93	9.43	11.49	11.95	9.65	10.71	7.54	7.93	9.68
RX5_laser meter	10.069	9.598	11.65	12.120	9.829	10.859	7.688	8.057	9.822
RX6_ruler	8.58	8.58	11.06	12.46	10.98	11.98	8.13	7.58	8.62
RX6_laser meter	8.742	8.730	11.24	12.588	11.144	12.153	8.282	7.753	8.754

A.3.2 Received signals

The following six figures are the receive signals of RX1 to RX6.

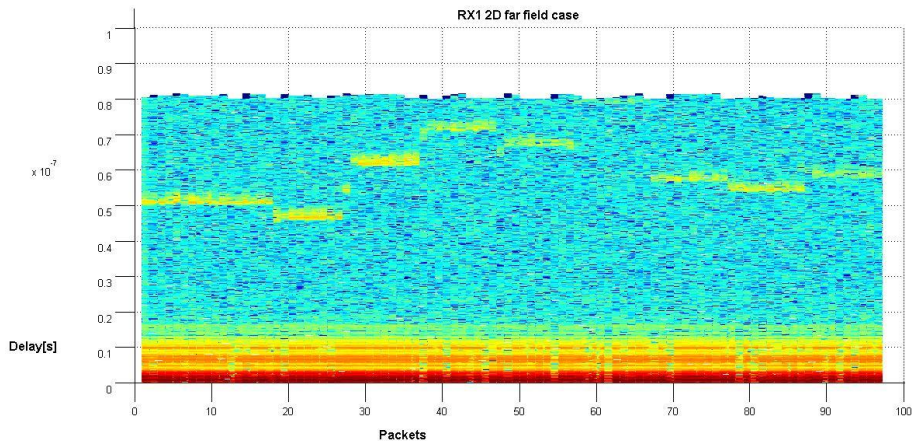


Figure 1. Received signals of RX1 | 2D far field.

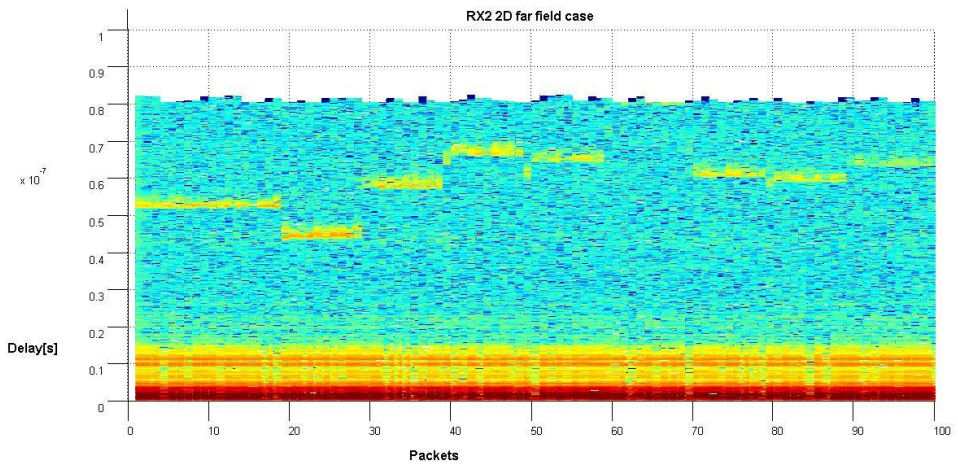


Figure 2. Received signals of RX2 | 2D far field.

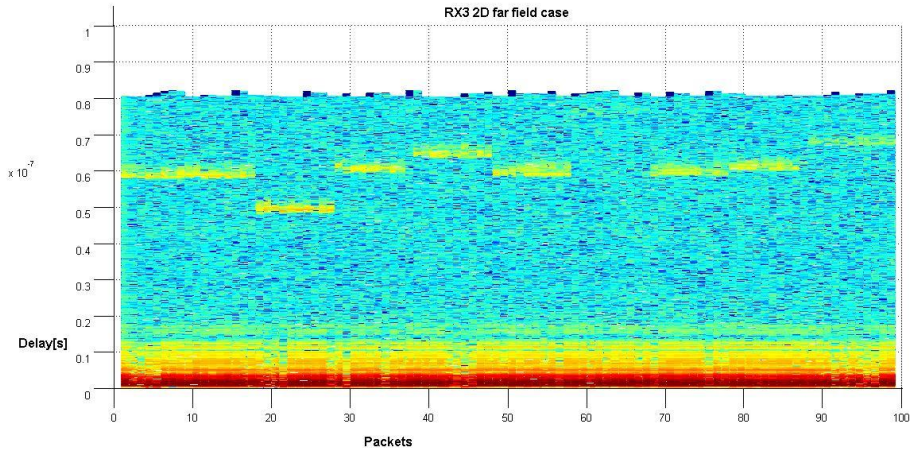


Figure 3. Received signals of RX3 | 2D far field.

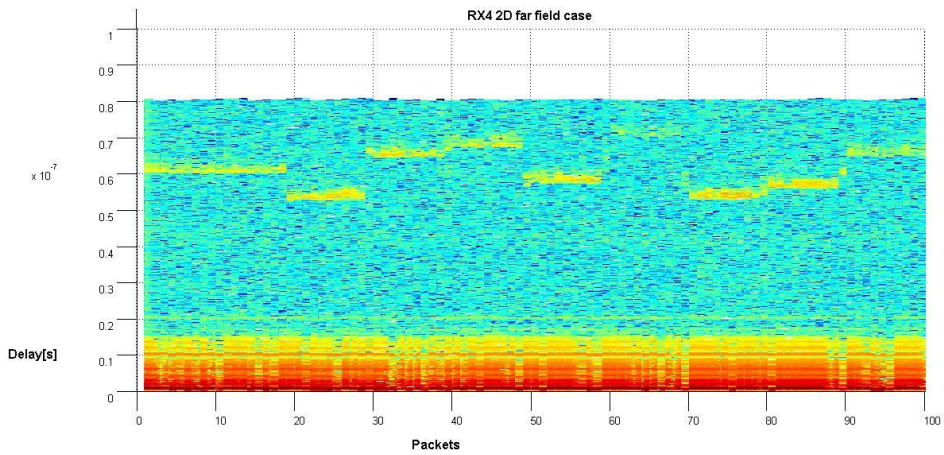


Figure 4. Received signals of RX4 | 2D far field.

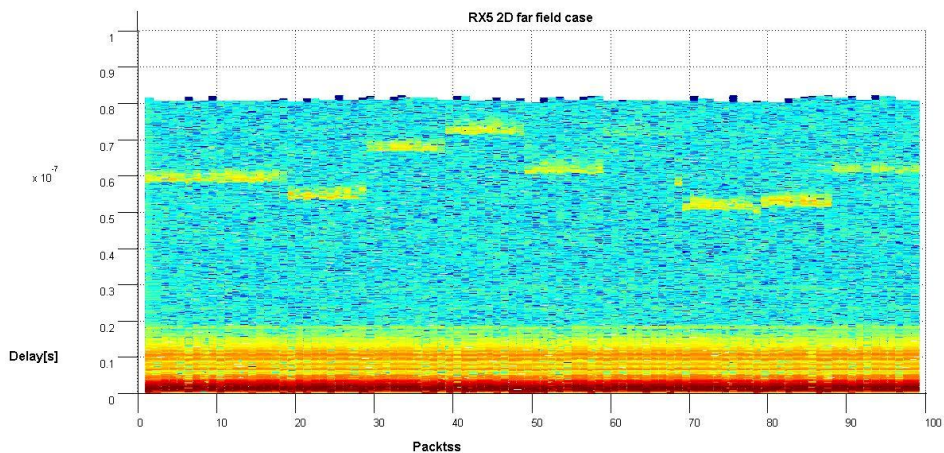


Figure 5. Received signals of RX5 | 2D far field.

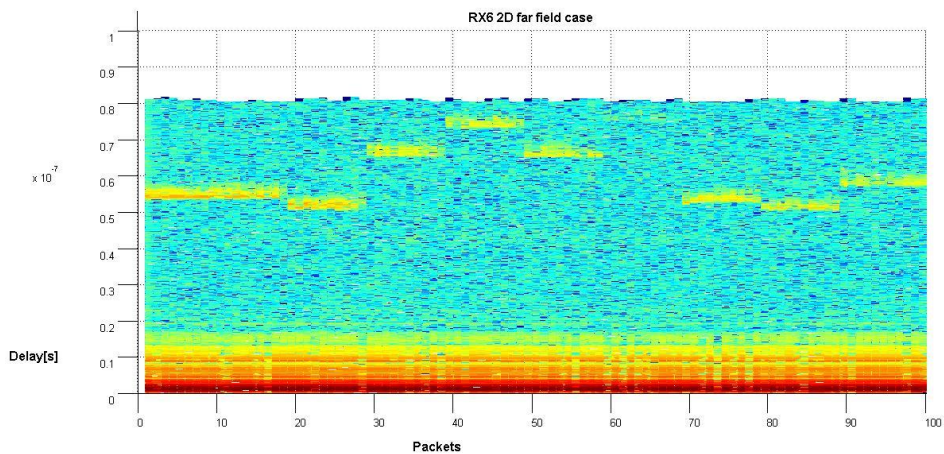


Figure 6. Received signals of RX6 | 2D far field.

A.3.3 Different distance

Table 7. Difference distance for RX1 (meters).

For RX1	Dd_ruler	Dd_laser	Dd_signal
S1	15,05	15,028	14.993
S2	13,73	13,768	13.777
S3	18,32	18,335	18.329
S4	21,33	21,27	21.228
S5	19,99	19,944	19.994
S6	23,68	23,59	None
S7	16,99	16,967	16.977

S8	16,13	16,108	16.117
S9	17,37	17,361	17.468

Table 8. Difference distance for RX2 (meters).

For RX2	Dd_ruler	Dd_laser	Dd_signal
S1	15,6	15,578	15.552
S2	13,05	13,088	13.061
S3	17,1	17,115	17.126
S4	19,88	19,82	19.782
S5	19,23	19,184	19.260
S6	23,81	23,72	None
S7	17,93	17,907	18.034
S8	17,52	17,498	17.647
S9	18,81	18,801	18.784

Table 9. Difference distance for RX3 (meters).

For RX3	Dd_ruler	Dd_laser	Dd_signal
S1	17,3	17,278	17.336
S2	14,41	14,448	14.451
S3	17,77	17,785	17.742
S4	19,06	19,0	18.918
S5	17,45	17,404	17.467
S6	22,36	22,27	None
S7	17,33	17,307	17.446
S8	17,84	17,818	17.967
S9	19,97	19,961	19.974

Table 10. Difference distance for RX4 (meters).

For RX4	Dd_ruler	Dd_laser	Dd_signal
S1	17,96	17,938	18.013
S2	15,74	15,778	15.772
S3	19,32	19,335	19.340
S4	20,24	20,18	20.151
S5	17,12	17,074	17.129
S6	21,08	20,99	None
S7	15,82	15,797	15.808
S8	16,66	16,638	16.705
S9	19,41	19,401	19.420

Table 11. Difference distance for RX5 (meters).

For RX5	Dd_ruler	Dd_laser	Dd_signal
S1	17,43	17,408	17.431
S2	15,93	15,968	15.916
S3	19,99	20,005	19.997
S4	21,45	21,39	21.315
S5	18,15	18,104	18.149
S6	21,21	21,12	None
S7	15,04	15,017	15.029
S8	15,43	15,408	15.445
S9	18,18	18,171	18.126

Table 12. Difference distance for RX6 (meters).

For RX6	Dd_ruler	Dd_laser	Dd_signal
S1	16,08	16,058	16.104
S2	15,08	15,118	15.106
S3	19,56	19,575	19.623
S4	21,96	21,9	21.886
S5	19,48	19,434	19.538
S6	22,48	22,39	None
S7	15,63	15,607	15.695
S8	15,08	15,058	15.155
S9	17,12	17,111	17.143

Appendix 4

A.4 Measured data and receive signals for 2D/3D far field case

A.4.1 Measured data

Following the description in Chapter 5, TX and Scatterers are kept in the same locations as the 2D far field test, thus most of the distances measured are the same as that in 2D far field case listed in appendix 3. Changes are the following three groups which are measured with the laser meter, 1) RX1/RX2/RX4/RX5 to Ref1/ Ref2; 2) TX to RX1/RX2/RX4/RX5; 3) RX1/RX2/RX4/RX5 to all scatterers. They are given in the table 1, 2, 3 and 4.

Table 1. The z-axis of RX1/RX2/RX4/RX5 measured by ruler and laser meter (meters).

	RX1	RX2	RX3	RX4	RX5	RX6
z-axis_ruler	3.86	3.18	0	2.26	1.21	0
z-axis_laser meter	3.995	3.316	0	2.425	1.358	0

Table 2. The distance from RX1/RX2/RX4/RX5 to Ref1/Ref2, measured by laser meter (meters).

	RX1	RX2	RX3 (unchanged)	RX4	RX5	RX6 (unchanged)
Ref1_laser meter	10.550	10.366		12.894	10.481	
Ref2_laser meter	10.848	10.852		10.823	11.662	

Table 3. The distance from RX1/RX2/RX4/RX5 to TX, measured by laser meter (meters).

	RX1	RX2	RX3 (unchanged)	RX4	RX5	RX6 (unchanged)
TX_lasermeter	4.233	3.624		1.974	2.886	

Table 4. The distance from RX1/RX2/RX4/RX5 to Scatterers (S1-S6), measured by laser meter (meters).

	S1	S2	S3	S4	S5	S6	S7	S8	S9
RX1_laser meter	8.669	8.270	10.565	12.358	12.076	13.771	10.269	9.535	9.760
RX2_laser meter	8.696	7.429	9.308	10.797	11.189	13.693	10.862	10.532	10.816
RX3 (unchanged)									
RX4_laser meter	10.819	9.651	11.115	10.977	8.948	10.829	8.631	9.467	11.208
RX5_laser meter	10.137	10.585	11.554	10.893	9.732	10.843	7.747	8.132	9.874
RX6 (unchanged)									

A.4.2 Receive signal

The following six figures are the receive signals of RX1, RX2, RX4, RX5 and RX6. The file of RX3 got damaged.

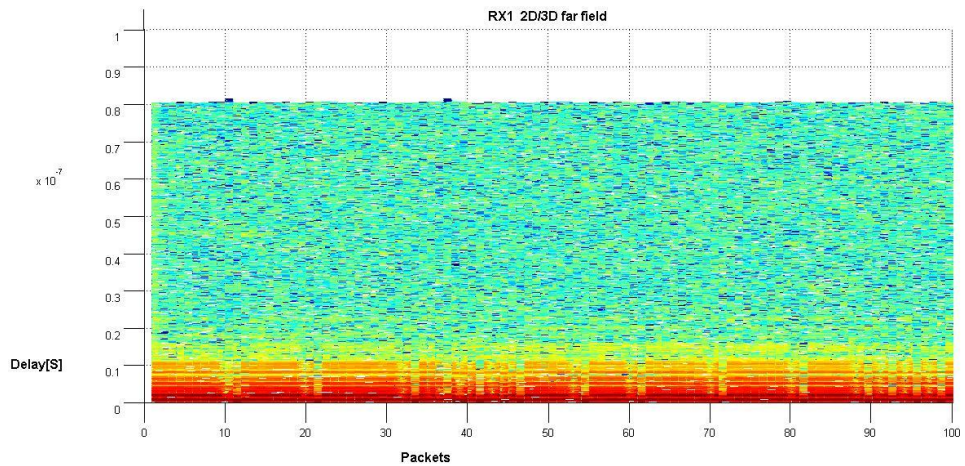


Figure 1. Received signals of RX1 | 2D/3D far field.

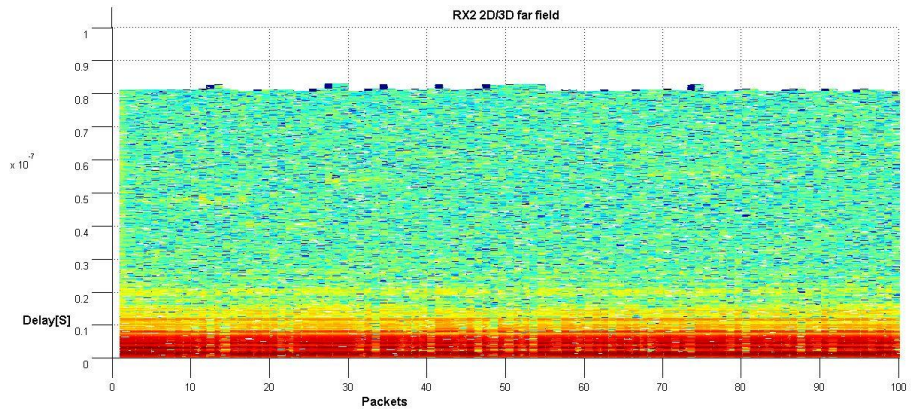


Figure 2. Received signals of RX2 | 2D/3D far field.

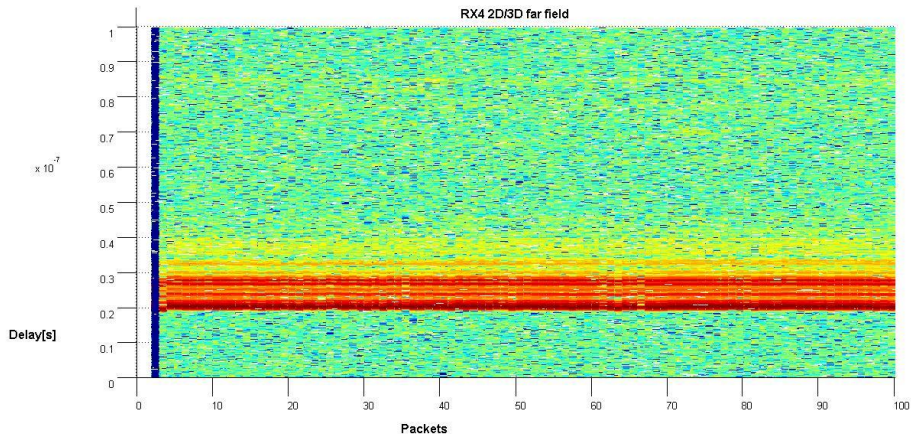


Figure 3. Received signals of RX4 | 2D/3D far field.

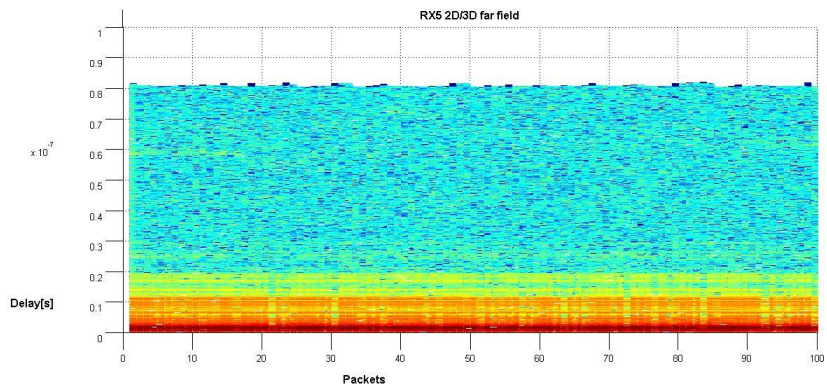


Figure 4. Received signals of RX5 | 2D/3D far field.

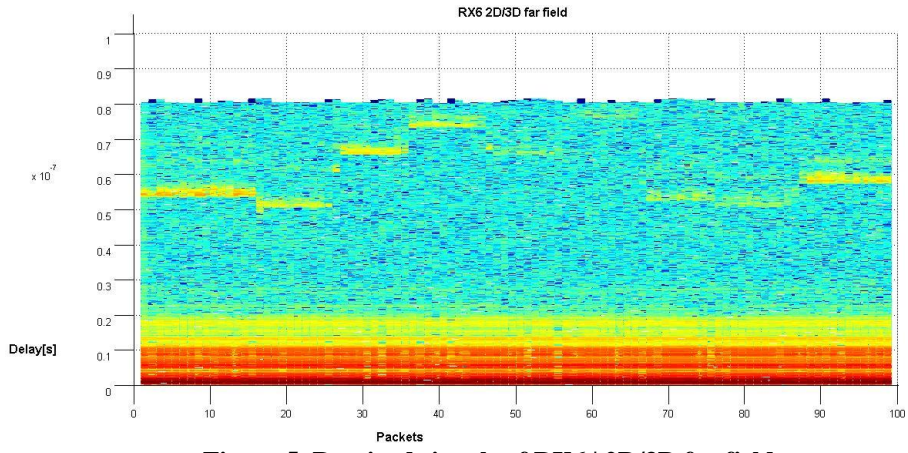


Figure 5. Received signals of RX6 | 2D/3D far field.